FORCE AND ENERGY MEASUREMENT OF BUBBLE-PARTICLE DETACHMENT

Hubert C.R. Schimann

Thesis submitted to the faculty of the Virginia Polytechnic Institute and State University
in partial fulfillment of the requirements for the degree of

Masters of Sciences
In
Mining and Minerals Engineering

R.H. Yoon
Tom Novak
Greg T. Adel
Gerald H. Luttrell

May 27, 2004
Blacksburg, Virginia

Keywords: coarse particle flotation, bubble-particle detachment, contact angle hysteresis, silica, octadecyltrichlorosilane, cetyltrimethylammonium bromide

FORCE AND ENERGY MEASUREMENT OF BUBBLE-PARTICLE DETACHMENT

by

Hubert C.R. Schimann

R.H. Yoon, Chairman

Mining and Minerals Engineering

(ABSTRACT)

Possibilities for increasing the upper limit of floatable particle sizes in the froth flotation process have been examined since the early beginnings of mineral flotation. The economic implications of such an increase are far ranging; from decreased grinding costs and increased recoveries to simplified flow-sheet design and increased throughput, all leading to increased revenue. Bubble-particle detachment has been identified as the main limiting factor for coarse particle flotation. The detachment process has been studied to better understand the factors influencing the strength of attachment and the energies involved. Direct measurements of bubble particle detachment were performed using a hanging balance apparatus (KSV Sigma 70 tensiometer) and using a submerged hydrophobic plate in water. Three experiments were used; direct force measurement of bubble-particle detachment, detachment force and energy of a bubble from a submerged hydrophobic plate, and detachment force and energy of a cetyltrimethylammonium bromide coated silica sphere from a flat bubble. Octadecyltrichlorosilane was used as a hydrophobic coating in the first two experimental methods. These experiments were recorded with a CCD camera to identify the detachment processes involved. Energies for both methods were calculated and divided into the two main steps of the detachment process: Three-Phase-Contact pinning and three phase contact line sliding. The first step represents the energy barrier which must be overcome before detachment can begin. It is directly related to contact angle hysteresis. Detachment occurs during the second step, where the solid-vapor interface is replaced by solid-liquid and liquid-vapor. This step

corresponds to the work of adhesion. The effects of surface tension, contact angle and hysteresis were well demonstrated with the three experimental methods. Good correlation was found between theoretical work of adhesion and measured energies.

ACKNOWLDEGEMENTS

First and foremost, the utmost appreciation is extended to my advisor Dr. Roe-Hoan Yoon, for his guidance, inspiration and support throughout the course of my investigations. The independence and freedom in choosing the direction to follow with my projects was also much appreciated. Special thanks are also extended to Dr. Jan Christer Eriksson (Department of surface chemistry, Royal Institute of Technology, Stockholm, Sweden) for the many conversations and advice which were instrumental in developing the ideas presented here. I am also grateful to Dr. Tom Novak, Dr. Gerald Luttrell, and Dr. Greg Adel who as members of my committee provided pertinent feedback. Special appreciation is given to Dr. Jinming Zhang, Jin Hong Zhang, and Jialin Wang for their helpful discussions, suggestions, friendship and willing assistance. Thanks are in order to Mariano Velázquez for his technical assistance and friendship.

I would also like to thank Dr. Dimetri Telionis and Dr. William Ducker for the courteous loan of equipment and lab space.

Particular thanks are in order to my lab mates Mr. Emílio Lobato, Mr. Ian Sherrell and Mr. Selahattin Baris Yazgan for all their helpful suggestions and continued support through all my ups and downs. I am most grateful for their friendships that were built over the past two years.

I owe special gratitude to Mr. Mert Kerem Eraydin for his friendship, continuous support and encouragements throughout my stay at Virginia Tech.

I would like to express my most sincere appreciation to my parents Monique and Karl Schimann for their inspiration, encouragements, wisdom, and continued suggestions. I would also like to thank my sister Erika and brother Michaël for their continued support throughout my two years here.

Finally I would like to express my deepest thanks to Mary-Joyce for all her encouragements, incredible patience, dedication and love. Mary-Joyce provided me with always cheerful inspiration, motivation and even technical assistance throughout my studies.

CONTENTS

LIST OF FIGURES

LIST OF TABLES

INTRODUCTION

Coarse particle flotation

Froth flotation is widely used in the mining industry to separate valuable minerals from other materials in their host environment. Minerals are separated by attaching themselves to rising air bubbles in the flotation cell and then recovered at the top of the cell. The ore must be ground small enough so that flotation can proceed (e.g. <.5 mm diameter). Coarse particle flotation provides opportunities for reduced grinding costs, increased recoveries and simplified flow-sheet designs (by eliminating certain classifying and other steps); all leading to increased throughput. However, the limits of coarse particle flotation have been well demonstrated as a severe decrease in recovery above a certain size with plant and laboratory batch tests data (Trahar 1981). A single bubble in a Hallimond tube was also used to demonstrate the dramatic drop in recovery with increasing particle size (Drzymala 1994). While other work identified a flotation domain from the minimum contact angle at which individual particle sizes will float (Crawford and Ralston 1988).

Flotation is a function of the probability of particle collection (Sutherland 1948)

$$P = P_C \cdot P_A \left(1 - P_D\right) \qquad [1]$$

where P_C, P_A, and P_D are the probabilities of collision, adhesion, and detachment respectively. The probability of collision depends on hydrodynamic effects in the flotation cell. The probabilities of adhesion and detachment are a combination of hydrodynamic effects and surface chemistry of the bubble and particle. Since surface chemistry is not affected by particle size, the probability of adhesion does not change much with particle size. Probability of detachment is then the main limiting factor in coarse particle flotation.

Research has focused on characterizing the various factors in flotation in attempts to increase the maximum floatable particle size. Early work identified the work of adhesion

$$W = T_{wa}\left(1 - \cos\theta\right) \qquad [2]$$

as the work done per unit area to create the air-solid interface at the expense of the solid-water interface (Wark 1933). Where T_{wa} is the surface tension of water and θ is the contact angle between the water and solid. Wark (1933) also attempted with limited success to calculate the maximum floatable particle size. The force and work required to remove a particle from the liquid-vapor interface was later measured using a centrifugal force apparatus and calculated as a function of the solid and liquid densities (Nutt 1960). Mathematical models of the flotation process followed taking into account the various sub-processes and physico-chemical properties involved in the system (Mika and Fuerstenau 1968). However, this model still suffered from a lack of proper description of these sub-processes to properly describe flotation. A theoretical evaluations of the upper particle size in flotation was calculated (Schulze 1977). These calculations were used to produce a rough estimation of the energy of rupture of a particle from a bubble. However, the work calculated in this manner does not represent an accurate description of the energy involved in the detachment process. A theoretical detachment force model was developed but disagreed by one order of magnitude when compared to forces measured using the centrifuge method (Nishkov and Pugh 1989).

More recent research on the stability of the bubble-particle aggregate in a flotation column using laboratory batch tests established some qualitative parameters for detachment energy of a particle from an oscillating bubble (Falutsu 1994). A bubble vibration detachment force measurement technique was developed to more closely resemble the conditions in flotation (Cheng and Holtham 1995), which compared favorably with previous theoretical work (Nutt 1960). Attachment and detachment efficiencies have also been described from calculation of the bubble-particle interaction forces in flotation and used to identify a maximum floatable particle size (Ralston et al. 1999).

Turbulent forces in the cell were recently modeled as the cause for bubble-particle detachment (Bloom and Heindel 2002; Pyke et al. 2003). Similarly, the detachment at the pulp-froth interface was described from experimental data by proposing an empirical model of percent apparent detachment during flotation (van Deventer et al. 2004). This later model compared attached and recovered particles to estimate the detachment.

Detachment force measurements

Direct measurements of detachment forces have been studied to better understand the detachment process and its implications for coarse particle flotation. Understanding of the detachment process holds the key to increasing the upper size limit of floatable particles. The detachment force of a particle from a bubble has been measured to correlate it with contact angle, and interfacial energy values (Janczuk 1983; Janczuk 1985; Janczuk et al. 1990). However, these all use controlled contact areas which prevent the bubble from freely spreading on the particle surface. This may represent some cases encountered in flotation but fails to accurately describe the overall interaction between bubbles and particles. A centrifuge method has also been used to measure the detachment force (Schulze et al. 1989). However, this method does not allow for observation of the detachment process, providing only a force range at which particle detachment occurred.

The atomic force microscope has provided an ideal method for measuring interactions between bubbles and individual colloidal particles(Butt 1994; Butt et al. 1995; Preuss and Butt 1998a; Preuss and Butt 1999). However, they have proved more useful for measuring interactions during the approach cycle than detachment. The amount of bubble deflection during detachment is difficult to accurately measure, thus the detachment cycle cannot by accurately described using this method.

The detachment models proposed above describe the detachment force with varying success, but do not accurately provide the detachment energy process. In the work

presented here, detachment forces were obtained using direct measurement methods and recorded by video to map the complete detachment process.

References

Adamson, A. W. (1997). *Physical Chemistry of Surfaces*, J. Wiley, New York.

Bloom, F., and Heindel, T. J. (2002). "On the structure of collision and detachment frequencies in flotation models." *Chemical Engineering Science*, 57(13), 2467-2473.

Butt, H.-J. (1994). "A Technique for Measuring the Force between a Colloidal Particle in Water and a Bubble." *Journal of Colloid and Interface Science*, 166(1), 109-117.

Butt, H.-J., Jaschke, M., and Ducker, W. (1995). "Measuring surface forces in aqueous electrolyte solution with the atomic force microscope." *Bioelectrochemistry and Bioenergetics*, 38(1), 191-201.

Byakova, A. V., Gnyloskurenko, S. V., Nakamura, T., and Raychenko, O. I. (2003). "Influence of wetting conditions on bubble formation at orifice in an inviscid liquid: Mechanism of bubble evolution." *Colloids and Surfaces A: Physicochemical and Engineering Aspects*, 229(1-3), 19-32.

Chatterjee, J. (2002). "Critical Eotvos numbers for buoyancy-induced oil drop detachment based on shape analysis." *Advances in Colloid and Interface Science*, 98, 265-283.

Cheng, T.-W., and Holtham, P. N. (1995). "The particle detachment process in flotation." *Minerals Engineering*, 8(8), 883-891.

Chibowski, E. (2003). "Surface free energy of a solid from contact angle hysteresis." *Advances in Colloid and Interface Science*, 103(2), 149-172.

Churaev, N. V., Ralston, J., Sergeeva, I. P., and Sobolev, V. D. (2002). "Electrokinetic properties of methylated quartz capillaries." *Advances in Colloid and Interface Science*, 96(1-3), 265-278.

Cohen, S. R., Naaman, R., and Sagiv, J. (1986). "Thermally induced disorder in organized organic monolayers on solid substrates." *J. Phys. Chem.*, 90, 3054-3056.

Crawford, R., and Ralston, J. (1988). "The influence of particle size and contact angle in mineral flotation." *International Journal of Mineral Processing*, 23, 1-24.

Datta, R. L., Napier, D. H., and Newitt, D. M. (1950). "The Properties and Behaviour of Gas Bubbles Formed at a Circular Orifice." *Trans. Inst. Chem. Eng.*, 28, 14 - 26.

DePalma, V., and Tillman, N. (1989). "Friction and wear of self-assembled trichlorosilane monolayer films on silicon." *Langmuir*, 5, 868-872.

Drzymala, J. (1994). "Characterization of materials by Hallimond tube flotation. Part 2: maximum size of floating particles and contact angle." *International Journal of Mineral Processing*, 42(3-4), 153-167.

Eckmann, D. M., and Cavanagh, D. P. (2003). "Bubble detachment by diffusion-controlled surfactant adsorption." *Colloids and Surfaces A: Physicochemical and Engineering Aspects*, 227(1-3), 21-33.

Eriksson, L. G. T., Claesson, P. M., Eriksson, J. C., and Yaminsky, V. V. (1996). "Equilibrium wetting studies of cationic surfactant adsorption on mica 1. Mono- and bilayer adsorption of CTAB." *Journal of Colloid and Interface Science*, 181, 476-489.

Eskilsson, K., and Yaminsky, V. V. (1998). "Deposition of monolayers by retraction from solution: Ellipsometric study of cetyltrimethylammonium bromide adsorption at silica-air and silica-water interfaces." *Langmuir*, 14, 2444-2450.

Falutsu, M. (1994). "Column flotation froth characteristics -- stability of the bubble-particle system." *International Journal of Mineral Processing*, 40(3-4), 225-243.

Frank, B., and Garoff, S. (1996). "Surfactant self-assembly near contact lines: control of advancing surfactant solutions." *Colloids and Surfaces A: Physicochemical and Engineering Aspects*, 116(1-2), 31-42.

Gun, J., Iscovici, R., and Sagiv, J. (1984). "On the formation and structure of self-assembling monolayers. II. A comparative study of Langmuir-Blodgett and adsorbed films using ellipsometry and IR reflection-absorption spectroscopy." *Journal of Colloid and Interface Science*, 101, 201-213.

Gun, J., and Sagiv, J. (1986). "On the formation and structure of self-assembling monolayers. III. Time of formation, solvent retention, and release." *Journal of Colloid and Interface Science*, 112, 457-472.

Hughes, R. R., Hanklos, A. E., Evans, H. D., and Maycock, R. L. (1955). "The Formation of Bubbles at Simple Orifices." *Chemical Engineering Progress*, 51(12), 557 - 563.

Huh, C., and Scriven, L. E. (1969). "Shapes of axysimmetric fluid interfaces of unbounded extent." *Journal of Colloid and Interface Science*, 35, 323.

Iimura, K.-i., and Kato, T. (2000). "Robustness of monolayers on the solids; comparative studies on thermal, solvent, pH, and mechanical resistance among 1-layer LB films of cadmium arachidate and alkylchlorosilanes." *Colloids and Surfaces A: Physicochemical and Engineering Aspects*, 171(1-3), 249-264.

Israelachvili, J. (1991). *Intermolecular & Surface Forces*, Elsevier Ltd., London.

James, D. F. (1974). "The meniscus on the outside of a small circular cylinder." *Journal of Fluid Mechanics*, 63(4), 657-664.

Janczuk, B. (1983). "The effect of n-alkanes on the force of air bubble detachment from a quartz surface in water." *Powder Technology*, 34(2), 243-247.

Janczuk, B. (1985). "Force of air bubble detachment from a quartz surface wetted with n-alkane in aqueous solutions of methanol and propanol." *Powder Technology*, 41(2), 106-112.

Janczuk, B., Wojcik, W., and Bialopiotrowicz, T. (1990). "Studies on contact angle and work of adhesion in the system coal/n-alkane film--air bubble--water." *Powder Technology*, 61(3), 211-216.

Janczuk, B., Wojcik, W., and Zdziennicka, A. (1999). "Wettability and surface free energy of glass in the presence of cetyltrimethylammonium bromide." *Materials Chemistry and Physics*, 58(2), 166-171.

Jones, S. F., Evans, G. M., and Galvin, K. P. (1999). "Bubble nucleation from gas cavities -- a review." *Advances in Colloid and Interface Science*, 80(1), 27-50.

Keen, G. S., and Blake, J. R. (1996). "A Note on the Formation and Rise of a Bubble from a Submerged Nozzle, Including Effects of Bulk- and Surface-Dilatational Viscosity." *Journal of Colloid and Interface Science*, 180(2), 625-628.

Li, C., and Somasundaran, P. (1992). "Reversal of Bubble Charge in Multivalent Inorganic Salt Solutions - Effect of Aluminum." *Journal of Colloid and Interface Science*, 148(2), 587-591.

Li, H. C. (1958). "Adsorption of organic and inorganic ions on quartz," PhD, Massachusetts Institute of Technology, Cambridge.

Li, H. Z., Mouline, Y., and Midoux, N. (2002). "Modelling the bubble formation dynamics in non-Newtonian fluids." *Chemical Engineering Science*, 57(3), 339-346.

Li, H. Z., and Quiang, S. (1998). "Formation des bulles dans les fluides newtoniens et non newtoniens." *Fluid Mechanics*, 326, 301-308.

Lin, J. N. (1994). "Role of interfacial tension in the formation and the detachment of air bubbles. 1. A single hole on a horizontal plane immersed in water." *Langmuir*, 10, 936-942.

Liu, J.-F., Min, G., and Ducker, W. (2001). "AFM study of adsorption of cationic surfactants and cationic polyelectrolytes at the silica-water interface." *Langmuir*, 17, 4895-4903.

Maoz, R., and Sagiv, J. (1984). "On the formation and structure of self-assembling monolayers. I. A comparative ATR-wettability study of Langmuir-Blodgett and adsorbed films on flat substrates and glass microbeads." *Journal of Colloid and Interface Science*, 100, 465-496.

Maoz, R., and Sagiv, J. (1987a). "Penetration-controlled reactions in organized monolayer assemblies. 1. Aqueous permanganate interaction with monolayer and multilayer films of long-chain surfactants." *Langmuir*, 3, 1034-1044.

Maoz, R., and Sagiv, J. (1987b). "Penetration-controlled reactions in organized monolayer assemblies. 2. Aqueous permanganate interaction with self-assembling monolayers of long-chain surfactants." *Langmuir*, 3, 1045-1051.

Mika, T. S., and Fuerstenau, D. W. "A microscopic model of the flotation process." *8th International Mineral Processing Congress*, Leningrad, U.S.S.R., 52.

Murray, B. S., Godfrey, J., Griesen, F., Healy, T., Lovelock, B., and Scales, P. (1991). "Spectroscopic and electrokinetic study of pH-dependent ionization of langmuir-blodgett films." *Langmuir*, 7, 3057-3064.

Nahra, H. K., and Kamotani, Y. (2003). "Prediction of bubble diameter at detachment from a wall orifice in liquid cross-flow under reduced and normal gravity conditions." *Chemical Engineering Science*, 58(1), 55-69.

Nishkov, I., and Pugh, R. J. (1989). "The relationship between flotation and adhesion of galena particles to the air-solution interface." *International Journal of Mineral Processing*, 25, 275-288.

Nutt, C. W. (1960). "Froth flotation: The adhesion of solid particles to flat interfaces and bubbles." *Chemical Engineering Science*, 12, 133-141.

Ouz, H., and Zeng, J. (1997). "Axisymmetric and three-dimensional boundary integral simulations of bubble growth from an underwater orifice." *Engineering Analysis with Boundary Elements*, 19(4), 319-330.

Parikh, A. N., Allara, D. L., Ben Azouz, I., and Rondelez, F. (1994). "An Intrinsic Relationship between Molecular Structure in Self-Assembled n-Alkylsiloxane Monolayers and Deposition Temperature." *J. Phys. Chem.*, 98, 7577-7590.

Parikh, A. N., Schivley, M. A., Koo, E., Seshadri, K., Aurentz, D., Mueller, K., and Allara, D. L. (1997). "n-Alkylsiloxanes: From Single Monolayers to Layered Crystals. The Formation of Crystalline Polymers from the Hydrolysis of n-Octadecyltrichlorosilane." *Journal of the American Chemical Society*, 119, 3135-3143.

Preuss, M., and Butt, H.-J. (1998a). "Direct measurement of particle-bubble interactions in aqueous electrolyte: dependence on surfactants." *Langmuir*, 14, 3164-3174.

Preuss, M., and Butt, H.-J. (1998b). "Measuring the Contact Angle of Individual Colloidal Particles." *Journal of Colloid and Interface Science*, 208(2), 468-477.

Preuss, M., and Butt, H.-J. (1999). "Direct measurement of forces between particles and bubbles." *International Journal of Mineral Processing*, 56(1-4), 99-115.

Pyke, B., Fornasiero, D., and Ralston, J. (2003). "Bubble particle heterocoagulation under turbulent conditions." *Journal of Colloid and Interface Science*, 265(1), 141-151.

Ralston, J., Fornasiero, D., and Hayes, R. (1999). "Bubble-particle attachment and detachment in flotation." *International Journal of Mineral Processing*, 56(1-4), 133-164.

Sagiv, J. (1980). "Organized monolayers by adsorption, 1. Formation and structure of oleophobic mixed monolayers on solid surfaces." *Journal of the American Chemical Society*, 102(1), 92-98.

Schulze, H. J. (1977). "New theoretical and experimental investigations on stability of bubble/particle aggregates in flotation: a theory on the upper particle size of floatability." *International Journal of Mineral Processing*, 4, 241-259.

Schulze, H. J., Wahl, B., and Gottschalk, G. (1989). "Determination of adhesive strength of particles within the liquid/gas interface in flotation by means of a centrifuge method." *Journal of Colloid and Interface Science*, 128(1), 57-65.

Shaw, D. J. (1992). *Introduction to colloid and surface chemistry*, Butterworth-Heinemann, Boston.

Silberzan, P., Leger, L., Ausserre, D., and Benattar, J. J. (1991). "Silanation of silica surfaces. A new method of constructing pure or mixed monolayers." *Langmuir*, 7, 1647-1651.

Sutherland, K. L. (1948). "Kinetics of the flotation process." *J. Phys. Chem.*, 52, 394-425.

Trahar, W. J. (1981). "A rational interpretation of the role of particle size in flotation." *International Journal of Mineral Processing*, 8, 289-327.

Tripp, C. P. (1991). "Reaction of chloromethylsilanes with silica: a low-frequency infrared study." *Langmuir*, 7, 923-927.

Tripp, C. P., and Hair, M. L. (1995). "Direct Observation of the Surface Bonds between Self-Assembled Monolayers of Octadecyltrichlorosilane and Silica Surfaces: A Low-Frequency IR Study at the Solid/Liquid Interface." *Langmuir*, 11, 1215-1219.

van Deventer, J. S. J., Feng, D., and Burger, A. J. (2004). "Transport phenomena at the pulp-froth interface in a flotation column: II. Detachment." *International Journal of Mineral Processing*, In Press, Corrected Proof.

van Oss, C. J. (1994). *Interfacial Forces in Aqueous Media*, Marcel Dekker, Inc., New York.

van Oss, C. J., Chaudhury, M. K., and Good, R. J. (1987). "Monopolar surfaces." *Advances in Colloid and Interface Science*, 28, 35-64.

Wark, I. W. (1933). "The physical chemistry of flotation. 1 The significance of contact angle in flotation." *Journal of Physical Chemistry*, 37, 623-644.

Wasserman, S. R., Tao, Y.-T., and Whitesides, G. M. (1989). "Structure and reactivity of alkylsiloxane monolayers formed by reaction of alkyltrichlorosilanes on silicon substrates." *Langmuir*, 5, 1074-1087.

Yaminsky, V. V. (1994). "Thermodynamic Analysis of Solute Effects on Surface Forces. Adhesion between Silicates in Solutions of Cationic Surfactants." *Langmuir*, 10, 2710-2717.

Yaminsky, V. V., and Ninham, B. W. (1999). "Surface forces vs. surface compositions. Colloid science from the Gibbs adsorption perspective." *Advances in Colloid and Interface Science*, 83(1-3 SU -), 227-311.

Yaminsky, V. V., and Yaminskaya, K. B. (1995). "Thermodynamic analysis of solute effects on contact angles. Equilibrium adsorption of cationic surfactants at silica-vapor and silica-water interfaces." *Langmuir*, 11, 936-941.

Yang, Z. L., Dinh, T. N., Nourgaliev, R. R., and Sehgal, B. R. (2001). "Numerical investigation of bubble growth and detachment by the lattice-Boltzmann method." *International Journal of Heat and Mass Transfer*, 44(1), 195-206.

Ye, S., Nihonyanagi, S., and Uosaki, K. (2001). "Sum frequency generation (SFG) study of the pH-dependent water structure on a fused quartz surface modified by an octadecyltrichlorosilane (OTS) monolayer." *Physical Chemistry Chemical Physics*, 3(16), 3643-3469.

Yiantsios S. G., and Karabelas A. J. (1995). "Detachment of Spherical Microparticles Adhering on Flat Surfaces by Hydrodynamic Forces." *Journal of Colloid and Interface Science*, 176(1), 74-85.

Zhao, X., and Kopelman, R. (1996). "Mechanism of organosilane self-assembled monolayer formation on silica studied by second-harmonic generation." *J. Phys. Chem.*, 100, 11014-11018.

Zhuravlev, L. T. (1987). "Concentration of hydroxyl groups on the surface of amorphous silicas." *Langmuir*, 3, 316-318.

Paper 1

Direct force and energy measurement of bubble-particle detachment

(pending publication)

Direct force and energy measurement of bubble-particle detachment

Hubert C.R. Schimann

Department of Mining and Minerals Engineering, Virginia Polytechnic Institute and State University, Blacksburg, VA, 24061, USA

Abstract

Bubble-particle detachment is the main limiting factor in coarse particle flotation. Detachment occurs when forces on the bubble-particle aggregate in a flotation cell overcome the strength of adhesion. Strength of adhesion depends on the particle surface roughness, surface chemistry, and surface tension of the liquid media. In the present work, detachment forces between spherical particles of varying hydrophobicity and air bubbles were directly measured using a modified KSV 70 surface tensiometer. The experiment was recorded with a 1 kHz CCD camera to monitor changes in bubble-particle contact area, bubble size and shape, and "neck formation". The detachment energy was found to consist of three parts; bubble stretching, bubble sliding, and bubble necking. The measured energies compared favorably to the work of adhesion.

Keywords: *detachment, bubble – particle interaction, coarse – particle flotation, octadecyltrichlorosilane*

Introduction

Froth flotation is widely used in the mining industry to separate valuable minerals from other materials in their host environment. Minerals are separated by attaching themselves to rising air bubbles in the flotation cell and then recovered at the top of the cell. The ore must be ground small enough so that flotation can proceed (e.g. <.5 mm diameter). Coarse particle flotation provides opportunities for reduced grinding costs, increased recoveries and simplified flow-sheet designs (by eliminating certain classifying and other steps); all leading to increased throughput.

Flotation is a function of the probability of particle collection (Sutherland 1948);

$$P = P_C \cdot P_A \left(1 - P_D\right) \quad [3]$$

where P_C, P_A, and P_D are the probabilities of collision, adhesion, and detachment respectively. The probability of collision depends on hydrodynamic effects in the flotation cell. The probabilities of adhesion and detachment are a combination of hydrodynamic effects and surface chemistry of the bubble and particle. Since surface chemistry is not affected by particle size, the probability of adhesion does not change much with particle size. Probability of detachment is then the main limiting factor in coarse particle flotation.

Theory

Flotation efficiency can be described largely in terms of contact angle or particle hydrophobicity. The equilibrium contact angle, θ_{Eq}, is the angle formed between a bubble and solid surface in water once the bubble becomes stable. It is described thermodynamically by Young's equation.

$$\frac{\gamma_{SV} - \gamma_{SL}}{\gamma_{LV}} = \cos\theta_{Eq} \quad [4]$$

Where, γ_{SV}, γ_{SL}, and γ_{LV} represent the solid-vapor, solid-liquid, and liquid-vapor interfacial tensions respectively. Where the liquid, vapor, and solid phases meet is referred to as the three-phase-contact (TPC) point or line. The interaction between two materials 1 (air) and 2 (solid) immersed in a third liquid 3 is given by (van Oss 1994);

$$\Delta G = \gamma_{SV} - \gamma_{SL} - \gamma_{LV} \quad [5]$$

Combining equations [4] and [5] leads to the Young-Dupré equation, which gives the free energy change for the attachment of a bubble onto a solid surface.

$$-\Delta G = \gamma_{LV}\left(1-\cos\theta\right) \qquad [6]$$

This represents the work required to remove liquid from the solid surface and bubble surface and create a new solid-vapor interface. This change in free energy is referred to as the work of adhesion since it represents the work required to form a bubble-particle aggregate. Calculating the actual energy spent requires the addition of an area term to equation [6] to account for the various initial and final interfacial areas. The thermodynamics of the bubble-article aggregate formation are reversible so that work of adhesion can be used to describe the energy required for detachment as well.

Bubble-particle detachment in flotation is mostly caused by turbulence in the cell. Once the forces on the particle are larger than the adhesion force, the particle detaches.

The detachment process depends on contact angle, media surface tension and surface heterogeneity or contact angle hysteresis. Contact angle determines the contact area between bubble and particle, which sets the distance that the TPC line will have to travel on the surface before detachment occurs. Surface tension corresponds to the tensile strength of the bubble.

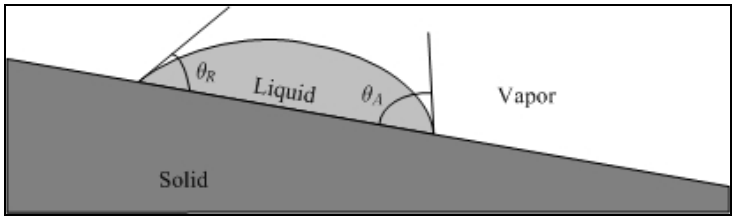

Figure 1 - Advancing and receding contact angle

Contact angle hysteresis has a role in determining the force and energy that must be overcome before the detachment process can begin. Hysteresis is caused by surface

roughness (Israelachvili 1991) and on a smaller scale by surface energy of the solid (Chibowski 2003). When a liquid drop moves on a surface, the angle formed at the side of the drop which is advancing on the surface is referred to as the advancing contact angle (see Figure 1). And reversely, the angle formed at the receding end is the receding contact angle. If a bubble is detached from a particle, the TPC will not move until the advancing contact angle is reached. At the higher contact angle the water can advance on the solid surface. The energy spent shifting the TPC from equilibrium to advancing angle represents energy barrier which must be overcome before the detachment process can begin. Alternatively, hysteresis also raises some questions about the reversibility of the work of adhesion. It is believed that during the recession process, the interface may not be retracing its original path, so that the process may not be thermodynamically reversible (Israelachvili 1991). This will be revisited in the results and discussion.

Surface tension is an important determining factor in bubble-particle adhesion and detachment. It determines the strength and elasticity characteristics of the bubble. A lower tension means a less 'stretchable' but stronger bubble. A more 'stretchable' bubble may require more energy, but less force to detach.

Experimental Methods

Forces were measured using a Sigma 70 surface tensiometer (KSV Instruments Ltd.). This equipment was a hanging balance with a resolution of 1μN. The bubble-particle interactions were recorded using a Phantom V4.0 CCD camera (Photo-Sonics Inc.). Interactions were also photographed by a 4.0M pixel S4 digital camera (Canon Inc.) equipped with a reversed 50mm AF NIKKOR (Nikon Corporation) lens (which allows it to act as a macro lens).

All the reagents used in the experiment were at least ACS grade and were obtained from either Fisher Scientific or Alfa Aesar. Soda lime glass spheres with a mean diameter of 2007μm ±40μm (Duke Scientific Corporation) were methylated with

octadecyltrichlorosilane (OTS) and butyltrichlorosilane (BTS) to create surfaces with varying hydrophobicity. The methylation procedure consists of washing the samples for 1hr in Piranha solution (30% H_2O_2:70% H_2SO_4) at 60-70°C. The samples are then rinsed in Nanopure water and immersed in a 10^{-5}M silane solution in toluene for 30-90 minutes depending on the target contact angle. The samples are then removed from solution and first rinsed with chloroform to remove any excess toluene from the surface, then acetone to remove any physisorbed silane. Following this, the samples are placed in acetone in an ultrasonic bath for at least 20min. This breaks up any amalgams of polymerized silane which may have accumulated at the silica surface, thereby creating a more uniform silane coating. The samples are stored in Nanopure water in sealed containers until the experiment.

A sphere was fixed to the end of a glass hook, which was manufactured by the Virginia Tech glass shop, using Crystalbond™ 509 glue (Electron Microscopy Sciences). The sphere was then suspended from the tensiometer above the bubble, which sat on the end of a thick glass rod (see Figure 2). The bubble support sat in a glass cell filled with water on top of a mechanical stage that could be moved vertically at 1mm/min to bring the bubble and particle into contact and then detach them.

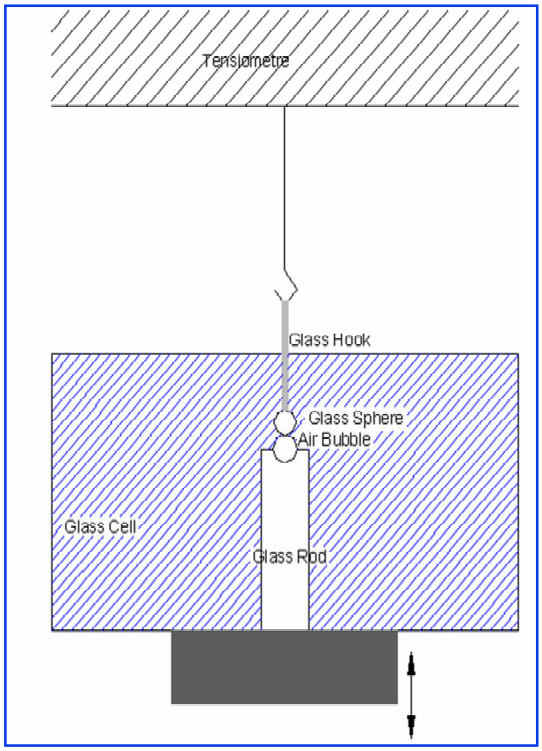

Figure 2 - Experimental apparatus

The tensiometer was connected to a computer to record force and distances every .25s. The reported distance is the relative position of the mechanical stage. Although the actual position is not known, the distance traveled during the detachment process (used for energy calculations) is still recorded.

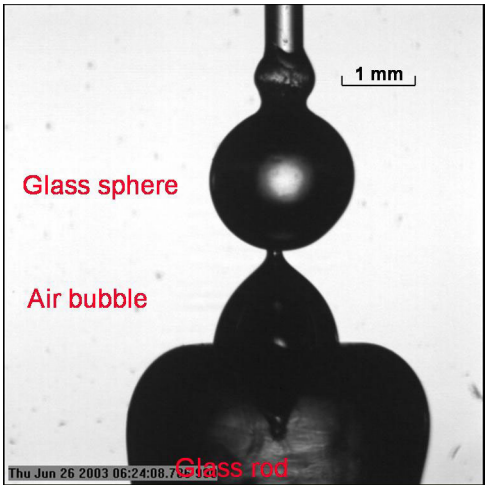

Figure 3 - Bubble-particle interaction

Figure 3 is a picture of the air bubble attached to its support as it is being pulled away from a glass sphere.

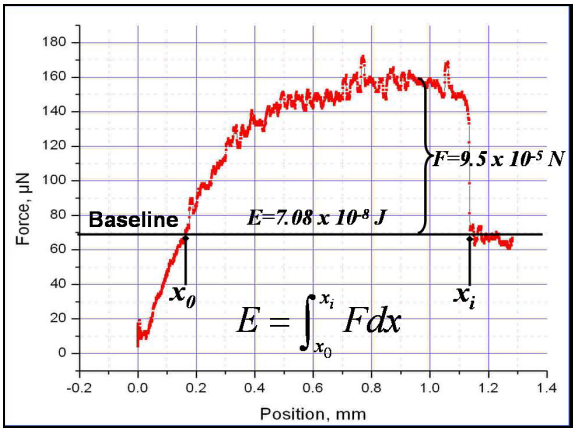

Figure 4 - Detachment force curve

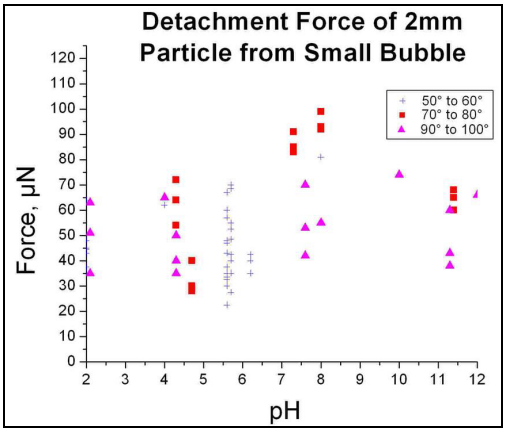

Figure 5 - Round bubble detachment force

A typical output curve from the surface tensiometer is shown in Figure 4. The detachment force is measured as the difference between the maximum and the baseline. The baseline is the force at which the sphere is detached. This is the force exerted on the instrument from the weight of the sphere only. The energy is taken as the integral of the force applied across the distance from equilibrium to detachment. Equilibrium is shown in the figure as x_0. It is the point at which the bubble is neither pushing up nor pulling down on the sphere.

Detachment force measurement between the sphere and bubble were not very reproducible when using a bubble of similar size as the sphere. Figure 5 displays force measurements performed under these conditions at varying contact angles.

In the next series of measurements, the small bubble was replaced by an infinitely large (or flat) bubble. The flat bubble removes the variations in bubble radius. The air bubble was created using a PTFE rod, with a cone bored out in the centre, connected to a syringe that provided the air for the bubble, see Figure 6.

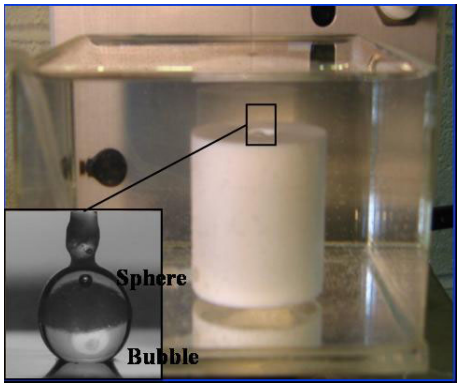

Figure 6 - Flat bubble apparatus

The flat bubble approach produced much more repeatable results as demonstrated in Figure 7. The CCD camera and digital camera were used to record the bubble-particle interactions to better understand the detachment mechanism.

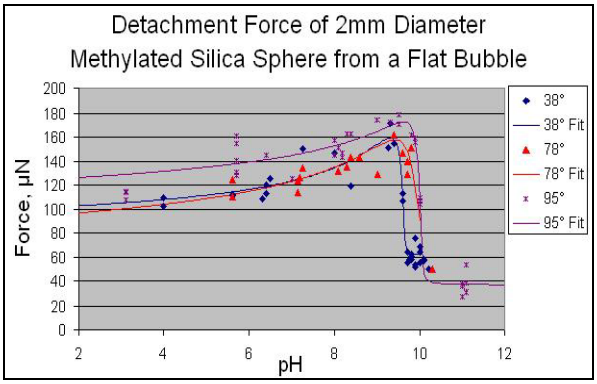

Figure 7 - Flat bubble detachment force

Results and Discussion

Detachment Mechanism

Bubble-particle detachment can be separated into two separate phases; E_1 and E_2; the bubble stretching, and the bubble detaching or sliding (Figure 8). The first phase is dependent on the chemical properties of the bulk solution, namely surface tension, and the second phase is dependent on the hydrophobicity of the particle.

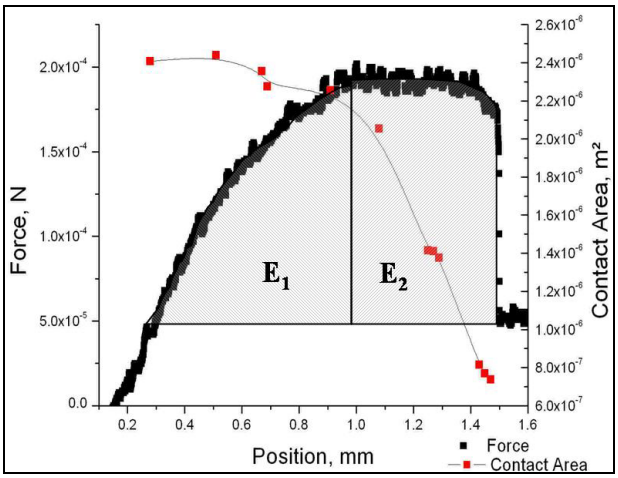

Figure 8 - Detachment force and contact area of methylated sphere from flat bubble (contact angle = 95°)

In the first component, the three-phase-contact (TPC) line is pinned on the silica surface while the bubble is being stretched. The bubble stretches until the advancing contact angle is reached. Surface roughness may cause the bubble to stretch slightly beyond this point. Once the advancing contact angle is reached, the vapor phase retracts from the sphere and the bubble commences detachment. The maximum force reached is dependent on the magnitude of the hysteresis and on surface tension of the media. Figure 8 demonstrates the two stages of the detachment process. Contact area remains constant (E_1) until enough force is applied to move the TPC line and the advancing contact angle has been reached. Once this occurs the force remains constant as the TPC line moves 'down' the sphere until detachment occurs.

The second component of the detachment process is dependent on particle hydrophobicity because this determines the starting contact area between solid and vapor. It also establishes a maximum, the advancing contact angle, which must be reached before movement of the TPC line can begin. Comparison of the different energy components with work of adhesion calculations further demonstrated this relationship.

Table 1 – Sphere-sphere energy of detachment and work of adhesion comparison

θ	48°	95°
E_1	1.824 x 10^{-2} J/m²	1.971 x 10^{-2} J/m²
E_2	1.794 x 10^{-2} J/m²	4.855 x 10^{-2} J/m²
E_{total}	3.618 x 10^{-2} J/m²	6.826 x 10^{-2} J/m²
W_a	1.367 x 10^{-2} J/m²	4.354 x 10^{-2} J/m²

Work of adhesion in the Table 1 was calculated from the differences in surfaces areas of the various interfaces between the initial attached and final detached states.

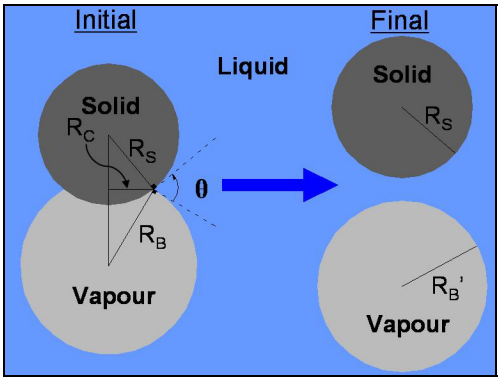

Figure 9 - Sphere-sphere work of adhesion calculation

The relationship is solved by assuming the vapor volume does not change from the initial to the final state. Solving the relationship gives the following equation for work of adhesion.

$$W_A = \frac{\Delta A_{LV}\gamma_{LV} + A_C\left(\gamma_{SL} - \gamma_{SV}\right)}{A_C} \qquad [7]$$

As can be seen from Table 1, the energy E_1, is fairly constant for 48° and 95° surfaces, because this portion of the detachment does not depend on the surface chemistry properties of the sphere. In mineral processing, this part of the detachment energy could be maximized using frother to create stronger bubbles. E_1 can also be regarded as an activation energy for detachment due to surface roughness and the magnitude dependent on the surface tension of the bulk solution in which the process takes place. E_2 shows

good correlation with the work of adhesion calculation because it is the actual energy of detachment whereas E_1 is the energy necessary to begin the detachment process.

Detachment Mechanism Model

Sphere and flat bubble detachment measurements provided a better insight into the detachment process, as bubble deformation was much more pronounced with the 'large' radius bubble. Figure 10 describes the bubble deformation geometry as the sphere is pulled away.

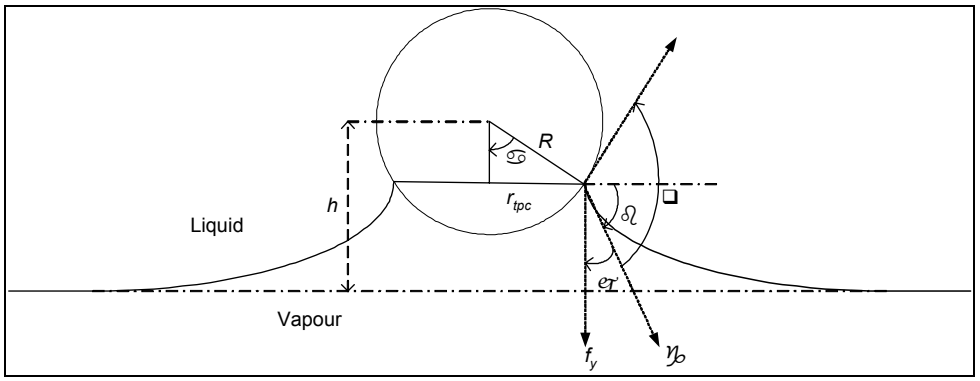

Figure 10 - Flat bubble - sphere detachment geometry

The air-water interface deformation as the sphere is pulled away from the bubble can be described by the following solution (Huh and Scriven 1969) to the Young-Laplace equation for capillarity.

$$\frac{d^2y}{dx^2} = \left[1+\left(\frac{dy}{dx}\right)^2\right]\left[\frac{\rho g}{\gamma}y\sqrt{1+\left(\frac{dy}{dx}\right)^2} - \frac{1}{x}\frac{dy}{dx}\right] \qquad [8]$$

where ρ is the density of the liquid, g is gravity, and γ is the interfacial tension.

Equation [8] can be solved numerically and leads to the following solution describing the height, h, of the TPC line above the flat bubble (James 1974).

$$h = R\sin\alpha\sin\beta\left[\ln\frac{4L}{R\sin\alpha(1+\cos\beta)} - \sigma\right]$$
$$L \equiv \sqrt{\frac{\gamma}{\rho g}} \qquad [9]$$

R is the radius of the sphere, L is the capillary length and σ is the Euler constant, 0.577. The force exerted by the bubble onto the sphere depends on the contact angle and shape of the bubble as these determine the angle at which the force is applied. The total force F exerted on the sphere in the vertical direction is

$$F = 2\pi R\sin\alpha\cdot\gamma_{LV}\cos\left(\frac{\pi}{2} - \theta + \alpha\right) \qquad [10]$$

When the sphere is at equilibrium position the bubble is not deformed and is not exerting any force on the sphere. The angle between the sphere and bubble at this point is the receding contact angle (Preuss and Butt 1998b), which can easily be calculated from the contact radius. As the sphere is pulled away, the shape of the bubble is defined by equation [8]. The contact angle is then calculated by solving equation [9] at progressing heights of the sphere above the bubble. Once the contact angle is known, and assuming a constant contact radius during the stretching portion of the detachment process, the force is calculated using equation [10] for each sphere height above the flat bubble datum. Force distance curves obtained in this manner were compared to the measured force curves, see Figure 11.

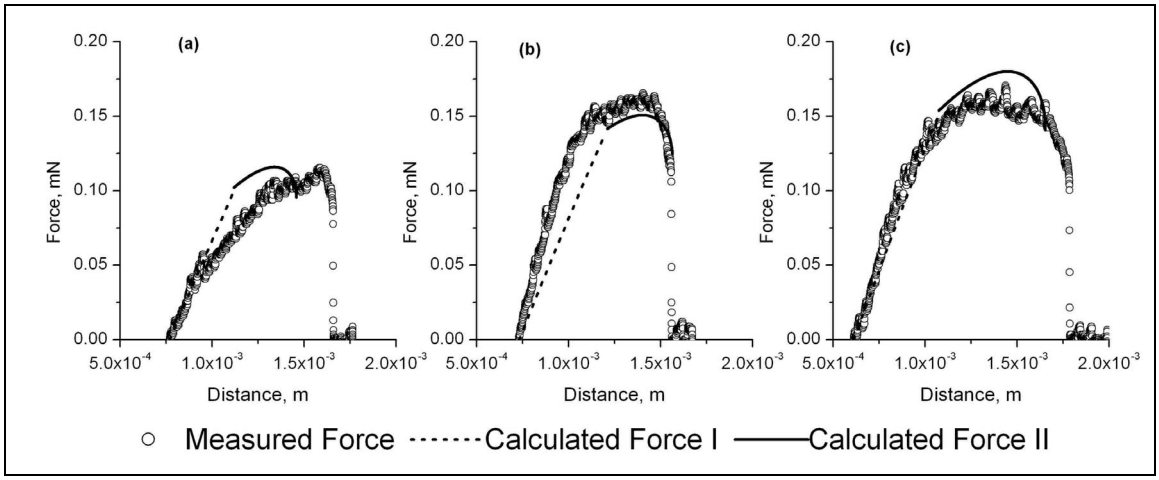

Figure 11 – Detachment force VS sphere center distance from the flat bubble for (a) 38° (b) 78° (c) 95° methylated silica spheres

'Calculated Force I' represents the stretching portion of the force curve calculated as described above. It represents the force exerted by the bubble on the sphere as the contact angle shifts from receding to advancing contact angle. 'Calculated Force I' shows good correlation with the measured force curve, although, graph (a) demonstrates some of the difficulty in simulating the detachment process. The experimental and calculated forces are in agreement for the first third of the curve, at which point the bubble seems to have 'slipped' on the sphere, causing a change in the slope due to the new contact radius.

Once the advancing contact angle is reached the bubble then begins sliding off the particle. This portion of the detachment curve was modeled by again solving equation [9] at progressing sphere heights, but now assuming that θ stays constant (note that $\theta = \alpha + \beta$). This portion of the detachment process is represented by 'Calculated Force II', which displayed good correlation with the measured force. Variation in this portion of the curve is probably due to the assumption that θ is constant. This is not entirely correct as the bubble will still experience some localized pinning on the sphere surface as it slides off. The calculated force also assumes a clean break instead of the necking behavior of the bubble seen at higher contact angles. Necking was observed during the experiment as contact angle increased, as evidenced by the small bubble often remaining

on the sphere after detachment, see Figure 12. This behavior is clearly visible when comparing graphs (a) and (c). In graph (a) there is almost no necking, so the measured force drops off abruptly at the end of the curve. The force curve in graph (c) slowly decreases before finally falling to zero.

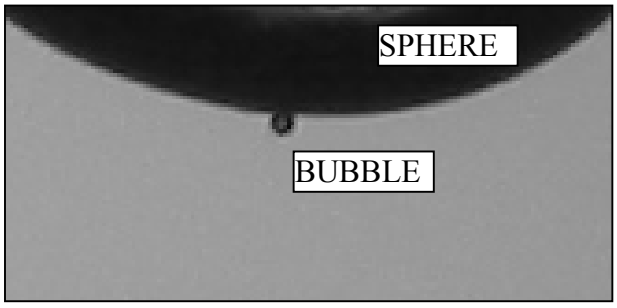

Figure 12 - Bubble on sphere surface after detachment

The measured energy was compared to the calculated work of adhesion for a sphere and flat bubble interaction. Work of adhesion was calculated with the following equation

$$W_A = \gamma_{LV}\pi R^2\left[\sin^2\theta_R - 2\cos\theta_{Eq}\left(1-\cos\theta_R\right)\right] \qquad [11]$$

where R is the radius of the sphere and θ_R and θ_{Eq} are the receding and equilibrium contact angles respectively. The work of adhesion calculation describes the change in free energies between the initial and final states as described in Figure 13.

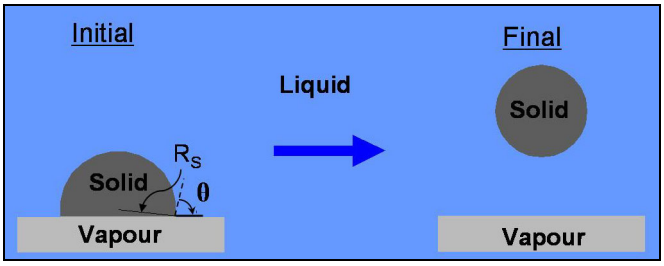

Figure 13 - Sphere - flat bubble work of adhesion calculation

Equation [11] assumes that the initial state is receding contact angle, and the equilibrium contact angle is used to cancel out the solid-liquid and solid-vapor interfacial tension

terms by means of Young's equation. If the angle at the initial stage is believed to equal equilibrium contact angle, then equation [11] reduces to the more commonly seen

$$W_A = \gamma_{LV} \pi R^2 \left(1 - \cos\theta\right)^2 \qquad [12]$$

Equation [12] for work of adhesion overestimates the energy of detachment with the difference between experimental and calculated increasing with contact angle. Equation [12] is also valid in the rare case where there is no contact angle hysteresis.

Work of adhesion (equation [11]) was compared to the measured energies of the detachment process. The experimental energy, E_2, was found to be similar to the work of adhesion, see Table 2 below.

Table 2 - Work of adhesion and experimental energy comparison

θ_R	θ_{Eq}	E_2, J	$E_{necking}$, J	E_2 - $E_{necking}$, J	W_A, J	% error
39.688	50.063	3.673E-08	7.771E-09	2.896E-08	2.560E-08	11.6%
43.118	56.588	5.970E-08	1.582E-08	4.387E-08	3.883E-08	11.5%
52.267	64.984	1.002E-07	2.972E-08	7.044E-08	6.800E-08	3.5%

However, if the energy of bubble necking as previously described is subtracted from E_2, then work of adhesion corresponds almost exactly to the measured energy (% error in the table is the error between W_A and E_2 minus the necking energy). This further supports the previous claim that E_2 represents the energy of detachment and E_1 is simply the energy barrier to detachment.

OTS Layer Modification With pH

The detachment force was measured over a wide pH range to observe its effect. This led to the finding of a pH dependence of the OTS layer on a silica surface. As pH in the bulk solution increases the hydrophobicity of the coating increases (see Figure 7). As the pH further increases, the detachment energy was observed dropping off drastically.

OTS was used because it forms a well ordered hydrophobic layer on the silicon surface (Cohen et al. 1986; Gun et al. 1984; Gun and Sagiv 1986; Maoz and Sagiv 1984; Maoz and Sagiv 1987a; Maoz and Sagiv 1987b). These OTS layers have been shown to be very resilient, resisting change in temperature, bulk solution chemistry, and even physical abrasion (DePalma and Tillman 1989; Iimura and Kato 2000). The adsorption reaction involves the formation of covalent bonds between the polar head group and $SiOH^-$ groups on the surface (Sagiv 1980; Tripp 1991; Tripp and Hair 1995; Zhao and Kopelman 1996). Polymerization between adsorbed sylil groups to form Si-O-Si networks has been reported (Zhao and Kopelman 1996). This seems unlikely due to the large space between ≡Si-OH groups on the surface (Zhuravlev 1987). Rather, the formation of –Si-O-Si- groups between OTS molecules and an adsorbed water layer on the quartz surface is more likely (Parikh et al. 1994; Parikh et al. 1997; Silberzan et al. 1991; Ye et al. 2001; Zhao and Kopelman 1996). This layer begins the ordering of the water molecules at the OTS coated surface, which is the nature of the hydrophobic behavior of the solid.

At acidic pH, the orientation of the water molecules at the substrate is reversed (Ye et al. 2001), which leads to a less ordered molecular structure of the water molecules in the bulk interface, thereby reducing the hydrophobic nature of the overall surface. This explains the slightly lower detachment force seen at acidic pH. As pH increases, detachment force increases until a peak at pH 9.5. The sudden drop following this peak is due to partial etching of the OTS layer at alkaline pH. IN the event of a 'perfect' monolayer, the molecules are packed too tight and prevent the penetration of OH^- ions. But etching can occur at defects in the OTS layer, and continues as more surface is uncovered (Iimura and Kato 2000; Wasserman et al. 1989). This explains the sharp drop in detachment force at alkaline pH.

The possibility of increased energy barrier with increasing pH has been analyzed as another source for the increase in detachment force and energy. OTS coated surfaces have been shown to behave similarly (electrokinetically) to bare silica with changing pH (Murray et al. 1991). In other words, the amorphous nature of silica is conserved on a coated surface.

The electrostatic bubble-particle interaction can be determined using the following relationship (Shaw 1992).

$$V_E = \frac{\pi\varepsilon_0\varepsilon R_1 R_2\left(\psi_1^2+\psi_2^2\right)}{4\left(R_1+R_2\right)}\left[\frac{2\psi_1\psi_2}{\psi_1^2+\psi_2^2}\ln\left(\frac{1+e^{-\kappa H}}{1-e^{-\kappa H}}\right)+\ln\left(1-e^{-2\kappa H}\right)\right] \qquad [13]$$

Where Ψ_1 and Ψ_2 represent the Stern potentials of the particle and air bubble of radii R_1 and R_2, respectively, ε is the dielectric constant of the medium, $1/\kappa$ the Debye length. Surface potential values from literature were used for the calculations (Li and Somasundaran 1992; Li 1958; Yiantsios S. G. and Karabelas A. J. 1995)

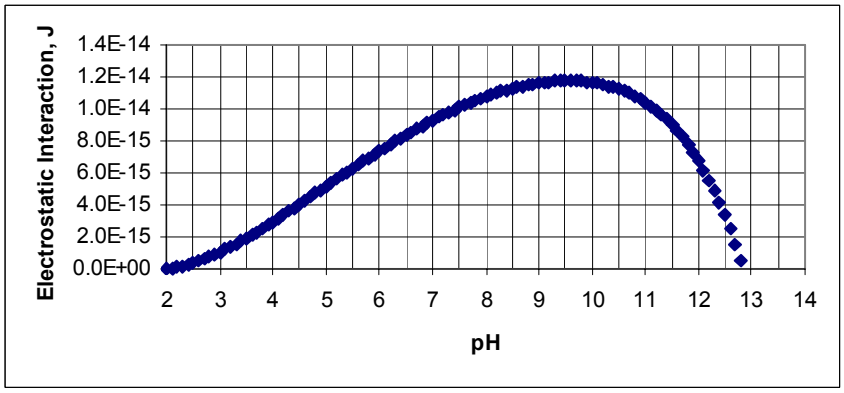

Figure 14 - Electrostatic interaction between a 2mm particle and a flat bubble

As Figure 14 indicates the peak repulsion is at pH 9.5. However, the interaction energy only amounts to 1.2 x 10^{-14} J, which is about 10^7 times lower than the interaction energies associated with these detachment processes. Thus, the energy of detachment variation at pH 9.5 is due to modification of the OTS layer and the water layer at the silica surface.

Summary & Conclusion

The Sigma 70 surface tensiometer was found to provide an accurate and reproducible method of measuring the force and energy of the bubble-sphere detachment process. Much better results were obtained when using a flat bubble, but this could be remedied (in the round bubble experiment) if extreme precaution was taken to ensure that a smaller bubble was the exact same size for each experiment.

Bubble-particle detachment is a three step process. The first step is the bubble stretching, which is directly related to surface tension and contact angle hysteresis. This also represents the energy barrier to detachment. The bubble stretching energy also corresponds to the energy required to move the three-phase-contact line. Once advancing contact angle is reached, the second step of detachment begins. The energy spent as the TPC line 'slides' off the particle is equivalent to the calculated work of adhesion. The third step of detachment is bubble necking. This part of the detachment process occurs as the ratio of contact radius to particle height above the flat bubble datum becomes too small to support a stable interface. Evidence of bubble necking increased with contact angle.

The complete detachment process can be modeled using numerical solutions to the Young-Laplace equation for vapor-liquid interface shape. The stretching portion of detachment is modeled by assuming that contact radius is constant and contact angle increases from receding to advancing. When advancing contact angle is reached the sliding and necking portions of detachment are modeled together assuming that contact angle is constant and contact radius is decreasing.

Silane coating of silica surfaces can be modified by pH. As pH increases, the hydrophobicity of the surface also increases until pH ≈9.5 due to modification of the water layer on the silica surface. Once pH increases past 9.5, the detachment energy decreases dramatically as the OTS layer is etched off the surface.

References

Chibowski, E. (2003). "Surface free energy of a solid from contact angle hysteresis." *Advances in Colloid and Interface Science*, 103(2), 149-172.

Cohen, S. R., Naaman, R., and Sagiv, J. (1986). "Thermally induced disorder in organized organic monolayers on solid substrates." *J. Phys. Chem.*, 90, 3054-3056.

DePalma, V., and Tillman, N. (1989). "Friction and wear of self-assembled trichlorosilane monolayer films on silicon." *Langmuir*, 5, 868-872.

Gun, J., Iscovici, R., and Sagiv, J. (1984). "On the formation and structure of self-assembling monolayers. II. A comparative study of Langmuir-Blodgett and adsorbed films using ellipsometry and IR reflection-absorption spectroscopy." *Journal of Colloid and Interface Science*, 101, 201-213.

Gun, J., and Sagiv, J. (1986). "On the formation and structure of self-assembling monolayers. III. Time of formation, solvent retention, and release." *Journal of Colloid and Interface Science*, 112, 457-472.

Huh, C., and Scriven, L. E. (1969). "Shapes of axysimmetric fluid interfaces of unbounded extent." *Journal of Colloid and Interface Science*, 35, 323.

Iimura, K.-i., and Kato, T. (2000). "Robustness of monolayers on the solids; comparative studies on thermal, solvent, pH, and mechanical resistance among 1-layer LB films of cadmium arachidate and alkylchlorosilanes." *Colloids and Surfaces A: Physicochemical and Engineering Aspects*, 171(1-3), 249-264.

Israelachvili, J. (1991). *Intermolecular & Surface Forces*, Elsevier Ltd., London.

James, D. F. (1974). "The meniscus on the outside of a small circular cylinder." *Journal of Fluid Mechanics*, 63(4), 657-664.

Li, C., and Somasundaran, P. (1992). "Reversal of Bubble Charge in Multivalent Inorganic Salt Solutions - Effect of Aluminum." *Journal of Colloid and Interface Science*, 148(2), 587-591.

Li, H. C. (1958). "Adsorption of organic and inorganic ions on quartz," PhD, Massachusetts Institute of Technology, Cambridge.

Maoz, R., and Sagiv, J. (1984). "On the formation and structure of self-assembling monolayers. I. A comparative ATR-wettability study of Langmuir-Blodgett and adsorbed films on flat substrates and glass microbeads." *Journal of Colloid and Interface Science*, 100, 465-496.

Maoz, R., and Sagiv, J. (1987a). "Penetration-controlled reactions in organized monolayer assemblies. 1. Aqueous permanganate interaction with monolayer and multilayer films of long-chain surfactants." *Langmuir*, 3, 1034-1044.

Maoz, R., and Sagiv, J. (1987b). "Penetration-controlled reactions in organized monolayer assemblies. 2. Aqueous permanganate interaction with self-assembling monolayers of long-chain surfactants." *Langmuir*, 3, 1045-1051.

Murray, B. S., Godfrey, J., Griesen, F., Healy, T., Lovelock, B., and Scales, P. (1991). "Spectroscopic and electrokinetic study of pH-dependent ionization of langmuir-blodgett films." *Langmuir*, 7, 3057-3064.

Parikh, A. N., Allara, D. L., Ben Azouz, I., and Rondelez, F. (1994). "An Intrinsic Relationship between Molecular Structure in Self-Assembled n-Alkylsiloxane Monolayers and Deposition Temperature." *J. Phys. Chem.*, 98, 7577-7590.

Parikh, A. N., Schivley, M. A., Koo, E., Seshadri, K., Aurentz, D., Mueller, K., and Allara, D. L. (1997). "n-Alkylsiloxanes: From Single Monolayers to Layered Crystals. The Formation of Crystalline Polymers from the Hydrolysis of n-Octadecyltrichlorosilane." *Journal of the American Chemical Society*, 119, 3135-3143.

Preuss, M., and Butt, H.-J. (1998). "Measuring the Contact Angle of Individual Colloidal Particles." *Journal of Colloid and Interface Science*, 208(2), 468-477.

Sagiv, J. (1980). "Organized monolayers by adsorption, 1. Formation and structure of oleophobic mixed monolayers on solid surfaces." *Journal of the American Chemical Society*, 102(1), 92-98.

Shaw, D. J. (1992). *Introduction to colloid and surface chemistry*, Butterworth-Heinemann, Boston.

Silberzan, P., Leger, L., Ausserre, D., and Benattar, J. J. (1991). "Silanation of silica surfaces. A new method of constructing pure or mixed monolayers." *Langmuir*, 7, 1647-1651.

Sutherland, K. L. (1948). "Kinetics of the flotation process." *J. Phys. Chem.*, 52, 394-425.

Tripp, C. P. (1991). "Reaction of chloromethylsilanes with silica: a low-frequency infrared study." *Langmuir*, 7, 923-927.

Tripp, C. P., and Hair, M. L. (1995). "Direct Observation of the Surface Bonds between Self-Assembled Monolayers of Octadecyltrichlorosilane and Silica Surfaces: A Low-Frequency IR Study at the Solid/Liquid Interface." *Langmuir*, 11, 1215-1219.

van Oss, C. J. (1994). *Interfacial Forces in Aqueous Media*, Marcel Dekker, Inc., New York.

Wasserman, S. R., Tao, Y.-T., and Whitesides, G. M. (1989). "Structure and reactivity of alkylsiloxane monolayers formed by reaction of alkyltrichlorosilanes on silicon substrates." *Langmuir*, 5, 1074-1087.

Ye, S., Nihonyanagi, S., and Uosaki, K. (2001). "Sum frequency generation (SFG) study of the pH-dependent water structure on a fused quartz surface modified by an octadecyltrichlorosilane (OTS) monolayer." *Physical Chemistry Chemical Physics*, 3(16), 3643-3469.

Yiantsios S. G., and Karabelas A. J. (1995). "Detachment of Spherical Microparticles Adhering on Flat Surfaces by Hydrodynamic Forces." *Journal of Colloid and Interface Science*, 176(1), 74-85.

Zhao, X., and Kopelman, R. (1996). "Mechanism of organosilane self-assembled monolayer formation on silica studied by second-harmonic generation." *J. Phys. Chem.*, 100, 11014-11018.

Zhuravlev, L. T. (1987). "Concentration of hydroxyl groups on the surface of amorphous silicas." *Langmuir*, 3, 316-318.

Paper 2

High-speed photographic studies of bubble formation, growth and detachment from hydrophobic surfaces

(pending publication)

High-speed photographic studies of bubble formation, growth and detachment from hydrophobic surfaces

Hubert C.R. Schimann

Department of Mining and Minerals Engineering, Virginia Polytechnic Institute and State University, Blacksburg, VA, 24061, USA

Abstract

Bubble particle detachment is the main limiting factor in coarse particle flotation. Detachment occurs when forces on the bubble-particle aggregate in a flotation cell overcome the strength of adhesion. Strength of adhesion depends on the particle contact angle, surface energy and roughness, and surface tension of the liquid media. Surface energy and roughness determine contact angle hysteresis, which causes the activation energy for detachment. Bubble detachment from a flat hydrophobic surface submerged in water was studied using a 1 kHz CCD camera. Images provided the data for thermodynamic and force calculations from the bubble shape size and movement on the plate. The measured energy of detachment was divided into the two parts: activation energy and work of adhesion. The measured work of adhesion compared favorably with calculated values.

Keywords: bubble detachment, octadecyltrichlorosilane, hysteresis, submerged plate

Introduction

Froth flotation is widely used in the mining industry to separate valuable minerals from other materials in their host environment. Minerals are separated by attaching themselves to rising air bubbles in the flotation cell and then recovered at the top of the cell. The ore must be ground small enough so that flotation can proceed (e.g. <.5 mm diameter). Coarse particle flotation provides opportunities for reduced grinding costs, increased recoveries and simplified flow-sheet designs (by eliminating certain classifying and other steps); all leading to increased throughput.

Flotation is a function of the probability of particle collection (Sutherland 1948);

$$P = P_C \cdot P_A \left(1 - P_D\right) \qquad [14]$$

where P_C, P_A, and P_D are the probabilities of collision, adhesion, and detachment respectively. The probability of collision depends on hydrodynamic effects in the flotation cell. The probabilities of adhesion and detachment are a combination of hydrodynamic effects and surface chemistry of the bubble and particle. Since surface chemistry is not affected by particle size, the probability of adhesion is mostly a function of hydrodynamics and increases with particle size. Probability of detachment is then the main limiting factor in coarse particle flotation.

Detachment of a bubble from a submerged plate has previously been studied using various methods such as the single hole plate or simply a submerged plate (Byakova et al. 2003; Eckmann and Cavanagh 2003; Jones et al. 1999; Li et al. 2002; Li and Quiang 1998; Nahra and Kamotani 2003). However, these studies do not adequately describe the detachment process with regards to a flotation application. Many others have also observed bubbles at a submerged capillary tip rather than a plate to study formation and detachment (Churaev et al. 2002; Keen and Blake 1996; Ouz and Zeng 1997; Yang et al. 2001). These do not properly describe detachment as seen in flotation as the bubble cannot spread past the boundaries of the capillary tip.

Theory

The detachment of an air bubble from a flat surface submerged in water is dependent on contact angle, surface energy of the solid and water surface tension. Contact angle determines the size of the contact area between bubble and surface. Surface tension may be regarded as a force vector along the bubble wall at the three phase contact (TPC) line. This surface tension multiplied by the contact perimeter represents the tenacity of the bubble adhesion onto the surface.

Surface energy of the solid (Eskilsson and Yaminsky 1998) and roughness determine contact angle hysteresis. Hysteresis is the difference between advancing and receding contact angle. When a water drop slides down a glass window, for example, the bottom part of the drop forms a larger contact angle (taken through the water, between the tangent to the drop wall and the glass surface) then the top part. The bottom portion is advancing on the glass surface and is said to be the advancing contact angle. The top portion is retreating and is said to be the receding contact angle. In the same fashion, when a bubble first attaches to a solid in water, the bubble spreads on the surface at the receding contact angle (water is receding from the surface). As the bubble detaches and the contact area shrinks it does so at the advancing contact angle. When the bubble is at steady state with the surface, neither spreading nor detaching, it is at equilibrium contact angle, which is the average of receding and advancing angles.

Detachment involves the shrinking of the contact area as the air bubble retreats from the surface. The TPC line must be at advancing contact angle for the initial inward movement to begin. Thus hysteresis plays a determining role along with contact angle in the detachment process.

The bubble contact diameter on a flat surface is dominated by the contact angle (Lin 1994). Subsequently, the final size of the bubble before detachment depends on surface energy of the solid, liquid interfacial tension, and contact angle. The contact angle as reported by (Lin 1994) was always 90° at detachment. However, the angle at detachment should be the advancing angle or slightly larger if the TPC line is moving very rapidly. The plate in this study represents a large smooth hydrophobic particle on which the TPC spreading is not limited by physical characteristics of the solid. The contact area is then controlled strictly by surface energy of the plate and interfacial tension of the media. The role of surface tension was thoroughly explained in experiments with oil drops on a submerged horizontal plate (Chatterjee 2002).

The forces acting on a bubble attached to a horizontal plate submerged in water are the buoyancy force and surface tension force. At high flow rates the bubble momentum also contributes to detachment, but this is not the case here. The buoyant force of the bubble must overcome the interfacial tension for detachment to proceed. Once the interfacial tension force is overcome, the TPC line shifts from equilibrium to advancing angle whence the bubble begins to retract from the surface until complete detachment.

Experimental Methods

All the reagents used in the experiment were at least ACS grade and were obtained from either Fisher Scientific or Alfa Aesar. The plate consisted of a 25.4 mm x 25.4 mm x 1.0 mm silicon wafer donated by the Virginia Tech Materials Science department. Holes (diameter = 0.6mm) were drilled through the center of these plates using an ultrasonic cutting machine. Plate surface roughness was measured to be about 0.5 nm by profiling the surface with an atomic force microscope. These plates were then methylated with octadecyltrichlorosilane (OTS) to create hydrophobic surfaces. The methylation procedure consists of washing the samples for 1hr in Piranha solution (30% H_2O_2:70% $H2SO_4$) at 60 – 70°C. The samples are then rinsed in Nanopure water and immersed in a 10^{-5}M silane solution in toluene for 30 – 90 minutes depending on the target contact angle. The samples are then removed from the solution and first rinsed with chloroform to remove any excess toluene from the surface, then acetone to remove any physisorbed silane. Following this, the samples are placed in acetone in an ultrasonic bath for at least 20 min. This breaks up any amalgams of polymerized silane which may have accumulated at the silica surface, thereby creating a more uniform silane coating. The samples are stored in Nanopure water in sealed containers until the experiment. The roughness of coated plates was also measured and was found to be less than 1 nm, indicating a consistent silane coating. The above method was used to produce plates with contact angles of 85°, 95°, and 97°. The surface energies of the plates were determined from contact angle measurements of formamide, diiodomethane and water on the surfaces, using the method as outlined by (van Oss et al. 1987).

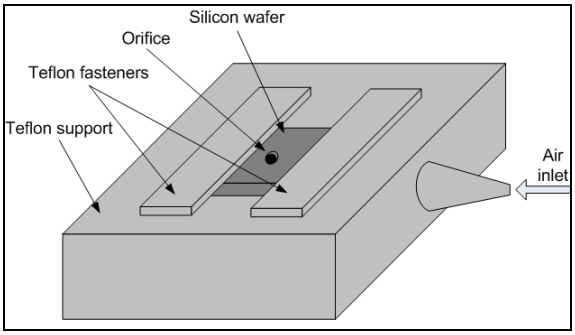

Figure 15 - Silicon plate support

The experiment involved submerging a horizontal plate with a hole drilled through the center in a water filled cell. The plate was attached to a Teflon support as shown in Figure 15, connected to an air source. Bubbles were produced at the orifice as air was fed through the system. The size of the orifice was kept constant, 0.6 mm diameter, as plates of different hydrophobicity were used. The size of the orifice has been shown to not affect the bubble characteristics as long as it is relatively small when compared to the bubble diameter (Datta et al. 1950). The relationship of cell size with bubble shape was also investigated and found to affect the bubble only under specific conditions which satisfy the following equation (Hughes et al. 1955)

$$v_c \approx \frac{A_0 \rho_g c^2}{g \Delta \rho} \qquad [15]$$

where, v_c is the cell volume, A_0 is the area of orifice, ρ_g is the gas density, c is the velocity of sound in the gas, g is the acceleration of gravity, and $\Delta\rho$ is the density difference between air and water. The cell used in this experiment was outside this range.

The experiments were recorded using a Phantom V4.0 CCD camera (Photo-Sonics Inc.) at 1000 frames per second. These digital images were analyzed to measure the bubble-surface contact area, dynamic contact angle, and bubble surface areas for thermodynamic

calculations. Using the images, detachment force from buoyancy of the volume of the bubble was measured.

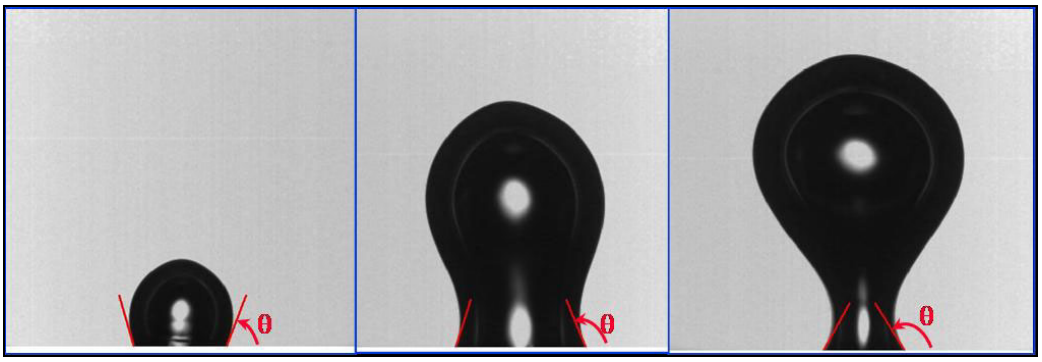

Figure 16 - Bubble at various stages of growth on flat plate

All the bubble measurements were made using MatLab (The MathWorks, Inc.) programs to analyze the images. Figure 16 shows an example of this analysis. The tangent to the bubble was traced at the contact to compute the instantaneous contact angle at each frame.

Results and Discussion

The experiments were limited to surfaces with contact angles larger than 90°, since below this the bubble does not instantaneously spread on the methylated surface. Bubble formation and detachment on the silicon wafer clearly demonstrated the importance of contact angle hysteresis in bubble-particle interactions. Figure 17 demonstrates the various stages of the interaction.

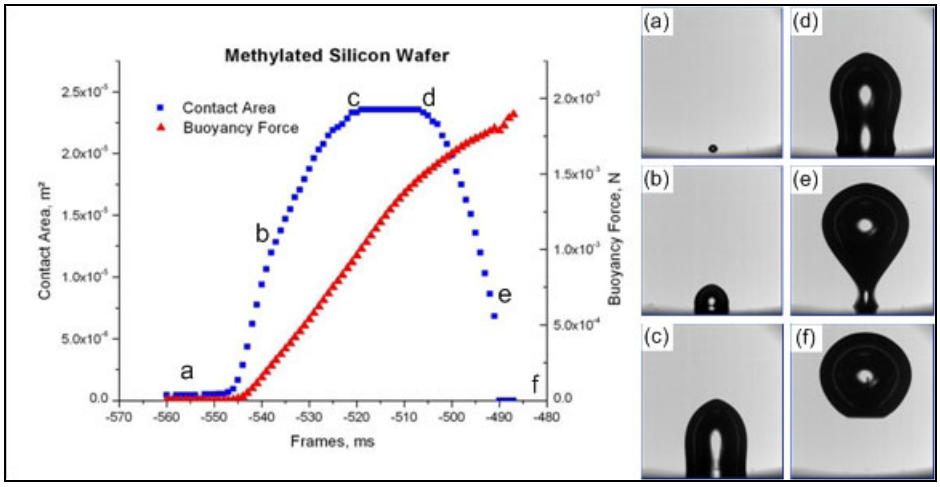

Figure 17 - Stages of bubble growth and detachment on methylated silicon wafer

In Figure 17(a) the bubble is still in the orifice, giving the reader an idea of the relative size of the hole compared to the contact area. As more air is fed through, the bubble wall breaks and attaches to the methylated surface in Figure 17(b). Here, the bubble forms the receding contact angle with the wafer as it spreads across the surface (i.e. water is receding from the surface). In Figure 17(c), the bubble has reached its maximum contact area. From this point on, the contact angle begins to increase until advancing contact angle is reached as shown in Figure 17(d). Once advancing contact angle is reached, water begins to advance on the silica surface. This is the beginning of the detachment process. Figure 17 (e) and (f) show the bubble as it is about to detach and once it has detached.

Between points (c) and (d), the buoyancy force keeps increasing. The energy spent during this time, while the contact area remains constant, is the energy required to shift the contact angle from receding to equilibrium and then advancing.

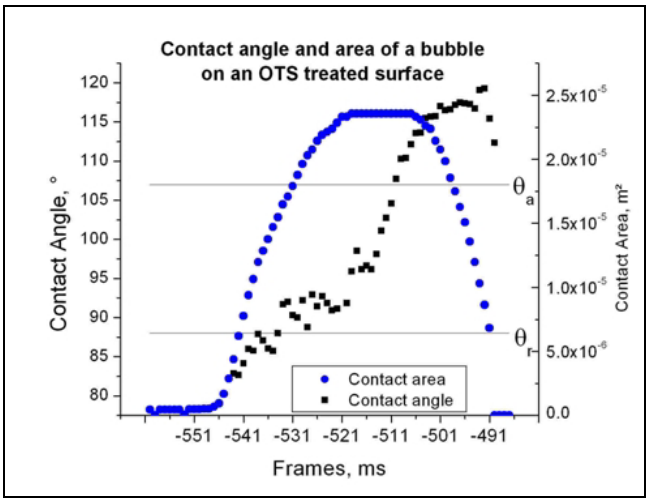

Figure 18 - Contact angle during growth and detachment process

The evolution of contact angle during the bubble spreading on and subsequent detachment from the wafer surface is further demonstrated in Figure 18. The bubble maintains receding contact angle during the contact area expansion. Then contact area decreases once the advancing contact angle has been reached. The energy spent shifting the TPC line from equilibrium angle to advancing to that detachment may begin represents activation energy or energy barrier to detachment. Because of the activation energy, work of adhesion is not a reversible process. The non-reversible nature of work of adhesion has been suggested previously (Israelachvili 1991) but only more recently demonstrated rigorously (Chibowski 2003).

Energy Calculations

Work of adhesion for the plate-sphere system was calculated to see how well it corresponded to the energies measured during the detachment process.

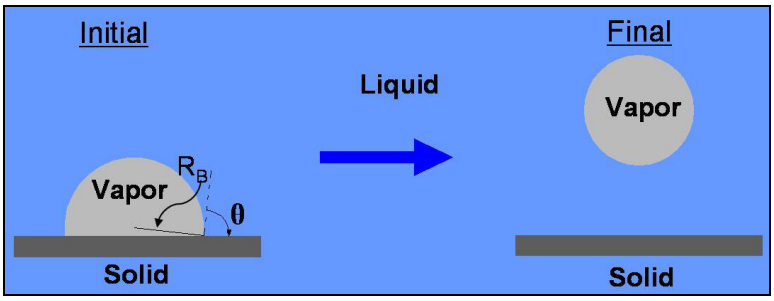

Figure 19 - Initial and final stages of bubble detachment

Figure 19 displays the initial and final energy states used to calculate the work of adhesion. The initial state represents the equilibrium state of the bubble and surface. Thus the bubble is at equilibrium contact angle with the surface. The work of adhesion calculation assumes that the bubble volume doesn't change between initial and final states. From this constant volume, the initial bubble radius, R_B was calculated using the final volume.

$$V = \frac{\pi}{6}\left[3R_C^2 + \left(R_B - \sqrt{R_B^2 - R_C^2}\right)^2\right]\left(R_B - \sqrt{R_B^2 - R_C^2}\right) \qquad [16]$$

Equation [16] determines the volume, V, of the bubble where R_B is bubble radius and R_C is the contact radius. The volume is then used in equation [17] to determine the change in liquid-vapor interface. Equation [18] is used to calculate the contact area as is represents the change in solid-vapor and solid-liquid interface.

$$\Delta A_{LV} = 4\pi\left(\frac{3V}{4\pi}\right)^{\frac{2}{3}} - 2\pi R_B\left(R_B - \sqrt{R_B^2 - R_C^2}\right) \qquad [17]$$

$$A_C = \pi R_B^2 \sin^2\theta \qquad [18]$$

$$W_A = \Delta A_{LV}\gamma_{LV} + A_C\left(\gamma_{SV} - \gamma_{SL}\right) \qquad [19]$$

Equation [19] calculates the work of adhesion (in Joules) for the system, where γ_{LV}, γ_{SV} and γ_{SL} are the liquid-vapor, solid-vapor, and solid-liquid interfacial tensions. The

volume of the bubble at equilibrium position was used to calculate the work of adhesion, which was compared with experimental detachment energy measurements.

The moving centroid method was used to measure the energy of the detachment. This method involves integrating the force applied by the bubble onto the surface over the distance traveled by the bubble centroid in the vertical direction, as shown in equation [21].

$$F_\gamma = 2\pi R_C \gamma_{LV} \sin\theta \qquad [20]$$

$$E = \int_{y_1}^{y_2} F_\gamma dy \qquad [21]$$

F_γ is the vertical component of the surface tension multiplied by the contact perimeter as shown in equation [20]. For the detachment process to begin F_B must overcome F_γ. Where, F_B represents the buoyancy force of the bubble.

When these two forces are equal the bubble is at equilibrium position and the bubble forms the equilibrium contact angle with the wafer surface. For the detachment process to begin, the TPC line must be shifted to advancing angle. E_1 is the activation energy required to shift the TPC line, and thereby begin the detachment process. The beginning of the detachment process is marked in Figure 20 by the sudden decrease in contact area. The energy spent from this point on until complete detachment represents the work of adhesion portion of the energy of detachment, E_2.

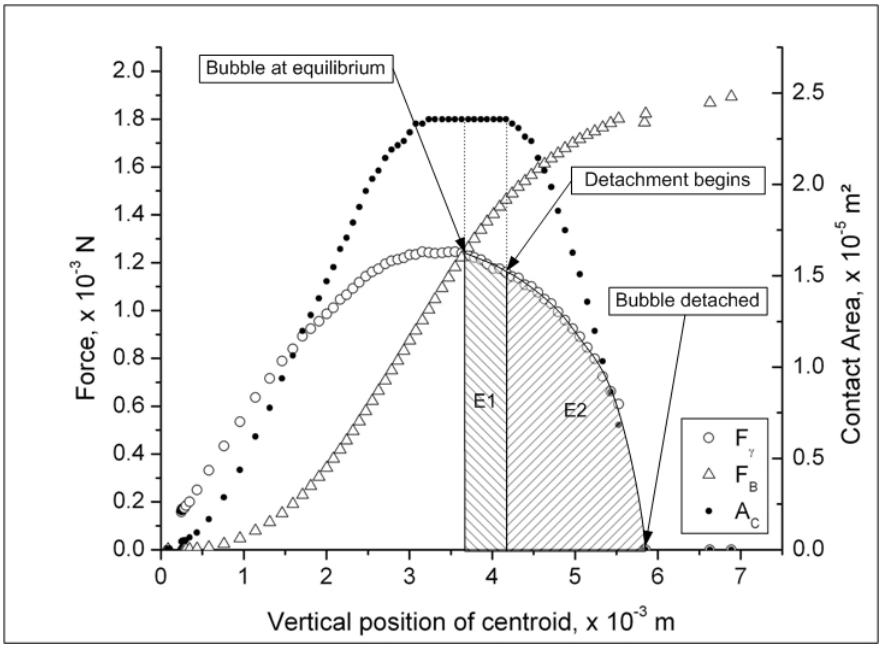

Figure 20 - Moving centroid method of energy of detachment calculation (θ = 97°)

Table 3 shows the energies calculated by the centroid method and how they compare to the work of adhesion calculated for these systems. As demonstrated, E_2 showed good correlation to the theoretical work of adhesion.

Table 3 – Moving centroid detachment energies and theoretical work of adhesion

Sample	I	II
Contact angle (hysteresis)	95° (32°)	97° (18°)
E_1	6.794 x 10^{-7} J	5.435 x 10^{-7} J
E_2	1.034 x 10^{-6} J	1.378 x 10^{-6} J
E_{total}	1.714 x 10^{-6} J	1.922 x 10^{-6} J
Theoretical W_A	1.132 x 10^{-6} J	1.325 x 10^{-6} J
% Error, (W_A vs E_2)	8.66%	4.00%

These measurements clearly demonstrate the importance of contact angle hysteresis. While sample II had a larger equilibrium contact angle, since sample I had more hysteresis, it required much more energy to detach.

Measured surface energies during the experiment provided a third method for energy of detachment determination. This method simply involves calculating the total surface free energy of the system for each frame in the experiment film. The energy difference

between equilibrium and complete detachment was then used as the energy of detachment.

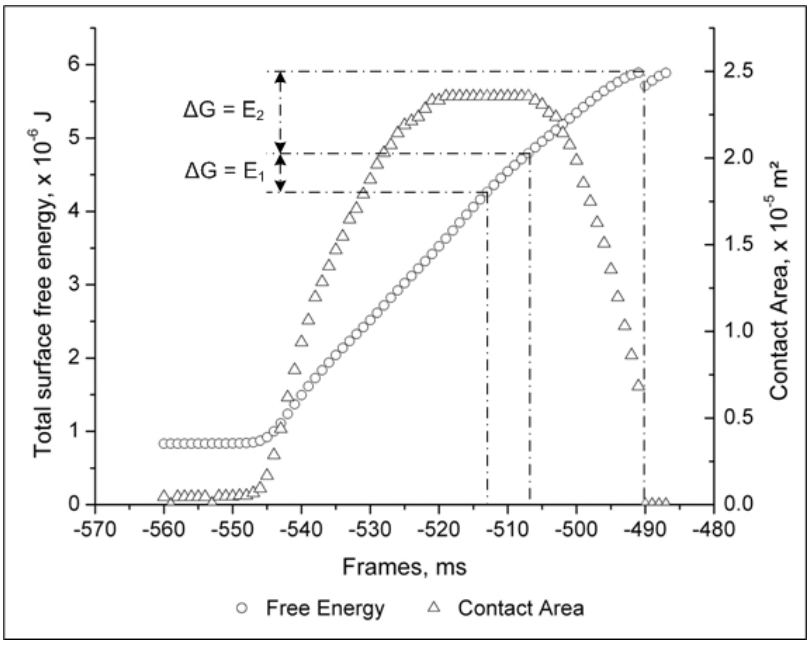

Figure 21 - Surface free energy of bubble and plate system

Figure 21 demonstrates the use of instant surface free energies to measure the energy of detachment. The free energy difference between equilibrium (frame -513) and beginning of detachment (frame -507) is equivalent to the activation energy, E_1. The free energy difference between beginning of detachment (frame -507) and complete detachment is equivalent to the work of adhesion or E_2. Note that at detachment the free energy dips slightly. This drop represents an exothermic process. Nature constantly seeks to reach lowest energy state. When detachment starts until one frame before detachment the free energy is increasing because an energy input is provided by the extra air being fed to the bubble. The instant before detachment, the bubble has reached its maximum stable size. This means that detaching rather than still growing allows the bubble to reach a lower energy state, thereby creating an instantaneous process.

Table 4 – Surface free energy detachment and theoretical work of adhesion

Sample	I	II
Contact angle (hysteresis)	95° (32°)	97° (18°)
E_1	7.863×10^{-7} J	5.279×10^{-7} J
E_2	9.924×10^{-7} J	1.097×10^{-6} J
E_{total}	1.779×10^{-6} J	1.625×10^{-6} J
Theoretical W_A	1.132×10^{-6} J	1.325×10^{-6} J
% Error, (W_A vs E_2)	12.33%	17.14%

The measured values shown in Table 4 again demonstrate the importance of contact angle hysteresis. Although sample I has a slightly smaller measured work of adhesion, E_2, it benefits from larger hysteresis, leading to larger activation energy, E_1, and ultimately a larger overall energy of detachment.

Summary & Conclusion

A submerged plate with a single orifice was successfully used to measure force and energy of detachment of a single bubble from a hydrophobic surface. The detachment force was obtained from buoyancy of the bubble, which was measured using image analysis of the experiment. Bubble equilibrium with the plate is reached when the buoyant force of the bubble is equivalent to the force due to surface tension.

Detachment energy was successfully measured using both the moving centroid method and surface free energy measurements also from image analysis. These methods clearly outlined the multiphase nature of the bubble detachment process. The first phase of detachment is shifting of the TPC line from equilibrium to advancing contact angle. The energy spent in doing so is referred to as the activation energy. The second phase occurs when the TPC slides inward until complete detachment. This subsequent component of the detachment process corresponds to the work of adhesion. Thus, if hysteresis is present the bubble-particle interaction is not a reversible process. The measured activation energy showed direct correlation to contact angle hysteresis and subsequent detachment energy corresponded closely to the calculated work of adhesion.

References

Byakova, A. V., Gnyloskurenko, S. V., Nakamura, T., and Raychenko, O. I. (2003). "Influence of wetting conditions on bubble formation at orifice in an inviscid liquid: Mechanism of bubble evolution." Colloids and Surfaces A: Physicochemical and Engineering Aspects, 229(1-3), 19-32.

Chatterjee, J. (2002). "Critical Eotvos numbers for buoyancy-induced oil drop detachment based on shape analysis." Advances in Colloid and Interface Science, 98, 265-283.

Chibowski, E. (2003). "Surface free energy of a solid from contact angle hysteresis." Advances in Colloid and Interface Science, 103(2), 149-172.

Churaev, N. V., Ralston, J., Sergeeva, I. P., and Sobolev, V. D. (2002). "Electrokinetic properties of methylated quartz capillaries." Advances in Colloid and Interface Science, 96(1-3), 265-278.

Datta, R. L., Napier, D. H., and Newitt, D. M. (1950). "The Properties and Behaviour of Gas Bubbles Formed at a Circular Orifice." Trans. Inst. Chem. Eng., 28, 14 - 26.

Eckmann, D. M., and Cavanagh, D. P. (2003). "Bubble detachment by diffusion-controlled surfactant adsorption." Colloids and Surfaces A: Physicochemical and Engineering Aspects, 227(1-3), 21-33.

Eskilsson, K., and Yaminsky, V. V. (1998). "Deposition of monolayers by retraction from solution: Ellipsometric study of cetyltrimethylammonium bromide adsorption at silica-air and silica-water interfaces." Langmuir, 14, 2444-2450.

Hughes, R. R., Hanklos, A. E., Evans, H. D., and Maycock, R. L. (1955). "The Formation of Bubbles at Simple Orifices." Chemical Engineering Progress, 51(12), 557 - 563.

Israelachvili, J. (1991). Intermolecular & Surface Forces, Elsevier Ltd., London.

Jones, S. F., Evans, G. M., and Galvin, K. P. (1999). "Bubble nucleation from gas cavities -- a review." Advances in Colloid and Interface Science, 80(1), 27-50.

Keen, G. S., and Blake, J. R. (1996). "A Note on the Formation and Rise of a Bubble from a Submerged Nozzle, Including Effects of Bulk- and Surface-Dilatational Viscosity." Journal of Colloid and Interface Science, 180(2), 625-628.

Li, H. Z., Mouline, Y., and Midoux, N. (2002). "Modelling the bubble formation dynamics in non-Newtonian fluids." Chemical Engineering Science, 57(3), 339-346.

Li, H. Z., and Quiang, S. (1998). "Formation des bulles dans les fluides newtoniens et non newtoniens." Fluid Mechanics, 326, 301-308.

Lin, J. N. (1994). "Role of interfacial tension in the formation and the detachment of air bubbles. 1. A single hole on a horizontal plane immersed in water." Langmuir, 10, 936-942.

Nahra, H. K., and Kamotani, Y. (2003). "Prediction of bubble diameter at detachment from a wall orifice in liquid cross-flow under reduced and normal gravity conditions." Chemical Engineering Science, 58(1), 55-69.

Ouz, H., and Zeng, J. (1997). "Axisymmetric and three-dimensional boundary integral simulations of bubble growth from an underwater orifice." Engineering Analysis with Boundary Elements, 19(4), 319-330.

Sutherland, K. L. (1948). "Kinetics of the flotation process." J. Phys. Chem., 52, 394-425.

van Oss, C. J., Chaudhury, M. K., and Good, R. J. (1987). "Monopolar surfaces." Advances in Colloid and Interface Science, 28, 35-64.
Yang, Z. L., Dinh, T. N., Nourgaliev, R. R., and Sehgal, B. R. (2001). "Numerical investigation of bubble growth and detachment by the lattice-Boltzmann method." International Journal of Heat and Mass Transfer, 44(1), 195-206.

Paper 3

Detachment of silica spheres from large air bubbles in cetyltrimethylammonium bromide solutions

(pending publication)

Detachment of silica spheres from large air bubbles in cetyltrimethylammonium bromide solutions

Hubert C.R. Schimann

Department of Mining and Minerals Engineering, Virginia Polytechnic Institute and State University, Blacksburg, VA, 24061, USA

Abstract

Bubble particle detachment is the main limiting factor in coarse particle flotation. Detachment occurs when forces on the bubble-particle aggregate in a flotation cell overcome its adhesive force. The strength of adhesion depends on contact angle, surface tension, and contact angle hysteresis. Detachment forces and energies were measured between a surfactant coated silica sphere and a flat bubble as a function of the surfactant concentration. A digital camera was used to measure the contact radius of the bubble on the sphere, to calculate the receding contact angle. The forces were used to calculate contact angles which were compared to Wilhelmy plate measurements on glass slides. The measured energy was separated into the energy barrier and the detachment energy which was compared to the theoretical work of adhesion.

Keywords: *Bubble-particle detachment force, cetyltrimethylammonium bromide, hysteresis*

Introduction

Froth flotation is widely used in the mining industry to separate valuable minerals from other materials in their host environment. Minerals are separated by attaching themselves to rising air bubbles in the flotation cell and then recovered at the top of the cell. The ore must be ground small enough so that flotation can proceed (e.g. <.5 mm diameter). Coarse particle flotation provides opportunities for reduced grinding costs, increased recoveries and simplified flow-sheet designs (by eliminating certain classifying and other steps); all leading to increased throughput.

Flotation is a function of the probability of particle collection (Sutherland 1948).

$$P = P_C \cdot P_A \left(1 - P_D\right) \qquad [22]$$

Where, P_C, P_A, and P_D are the probabilities of collision, adhesion, and detachment respectively. The probability of collision depends on hydrodynamic effects in the flotation cell. The probabilities of adhesion and detachment are a combination of hydrodynamic effects and surface chemistry of the bubble and particle. Since surface chemistry is not affected by particle size, the probability of adhesion is mostly a function of hydrodynamics and increases with particle size. Probability of detachment is then the main limiting factor in coarse particle flotation.

Cationic surfactants such as cetlytrimethylammonium bromide (C_{16}TAB) easily attach to the negatively charged silica surface. The C_{16}TAB molecules attach to the silanol groups at the glass surface which provide the negative sites. The sphere becomes more hydrophobic as more surfactant is adsorbed onto the surface. The density of the silanol groups determines the maximum possible C_{16}TAB density on the surface. As these negative sites are filled the surface is neutralized. The surfactant concentration where this occurs is the point of zero charge (pzc). Further C_{16}TAB adsorption occurs as concentration is increased through attraction between the hydrophobic tails. This creates a densely packed second layer on the sphere with the polar heads pointing toward solution, thereby decreasing the overall hydrophobicity of the sphere. Increasing the C_{16}TAB concentration also decreases the surface tension of the aqueous solution. This is similar to increasing the frother concentration in a flotation cell.

Theory

Detachment force

The total force exerted by the flat bubble onto the sphere is a function of the contact radius and angle formed at the interface. Figure 22 illustrates the geometry involved in the force equation derivation.

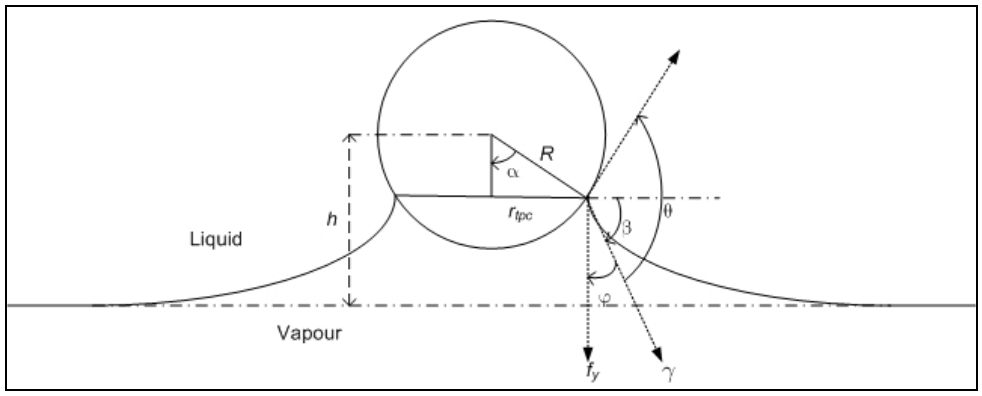

Figure 22 - Flat bubble - sphere detachment geometry

$$F = 2\pi r_{tpc}\gamma_{lv}\cos\varphi \qquad [23]$$

Equation [23] calculates the total force exerted by the bubble onto the sphere in the vertical direction due to surface tension, where γ_{lv} is the surface tension. The contact radius, r_{tpc}, is a function of the receding contact angle, θ_r. When the sphere first penetrates the bubble, water recedes from the solid surface. The TPC spreads on the solid until it is pinned at the radius of contact and settles at receding contact angle (Preuss and Butt 1998b). From Figure 22 it can be seen that the angle between the tangent at the contact line and the horizontal is equal to α. Thus, $r_{tpc} = R\sin\theta_r$. The TPC line stays pinned until advancing contact angle is reached. At advancing contact angle, $\varphi = \pi/2 - \theta_a + \theta_r$. The total force necessary to move the TPC on the sphere surface is then

$$F = 2\pi R\sin\theta_r \cdot \gamma_{lv}\cos\left(\frac{\pi}{2} - \theta_a + \theta_r\right) \qquad [24]$$

Work of adhesion

The measured energy was compared to the calculated work of adhesion for a sphere and flat bubble interaction. Work of adhesion was calculated with the following equation:

$$W_A = \gamma_{LV}\pi R^2\left[\sin^2\theta_R - 2\cos\theta_{Eq}\left(1-\cos\theta_R\right)\right] \quad [25]$$

where R is the radius of the sphere and θ_R and θ_{Eq} are the receding and equilibrium contact angles respectively. The work of adhesion calculation describes the change in free energies between the initial and final states as described in Figure 13.

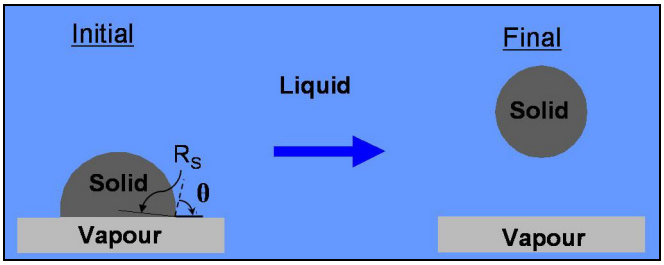

Figure 23 - Sphere - flat bubble work of adhesion calculation

Equation [11] assumes that the initial state is receding contact angle, and the equilibrium contact angle is used to cancel out the solid-liquid and solid-vapor interfacial tension terms by means of Young's equation. If the angle at the initial stage is believed to equal equilibrium contact angle, then equation [11] reduces to the more commonly seen

$$W_A = \gamma_{LV}\pi R^2\left(1-\cos\theta\right)^2 \quad [26]$$

Equation [12] for work of adhesion overestimates the energy of detachment with the difference between experimental and calculated increasing with contact angle. Equation [12] is also valid in the rare case where there is no contact angle hysteresis.

Equations [24] and [11] illustrate the importance of contact angle hysteresis in the detachment process. Hysteresis is caused by surface roughness (Adamson 1997; Israelachvili 1991) and by surface energy of the solid (Chibowski 2003). The C_{16}TAB molecules adsorb onto the silica surface in patches or domains, thereby creating chemically heterogeneous surfaces than can lead to increased hysteresis.

Surfactant adsorption at the solid-liquid-vapor interface during movement of the solid across the liquid vapor interface can also cause hysteresis. During Wilhelmy plate measurements of advancing and receding contact angles, a surfactant coated plate is introduced vertically into aqueous surfactant solution. The liquid vapor boundary depresses as the solid is pushed down past the water surface. The meniscus created by this depression will form the advancing contact angle with the plate, and remain at that angle as the plate is lowered further into the solution. CTAB molecules in the solution will orient themselves at the TPC so as to have the hydrophobic tail onto the solid to escape the water (Yaminsky and Ninham 1999). This phenomenon leads to increased pinning of the TPC line and consequently larger advancing contact angles.

Experimental Methods

Forces were measured using a Sigma 70 Surface tensiometer (KSV Instruments Ltd.). This equipment was a hanging balance with a resolution of 1 μN. The bubble-particle interactions were photographed by a 4.0M pixel S4 digital camera (Canon Inc.) equipped with a reversed 50 mm AF NIKKOR (Nikon Corporation) lens (which allows it to act as a macro lens).

Soda lime glass spheres with a mean diameter of 2007 μm ± 40 μm (Duke Scientific Corporation) were used in the experiment. The diameter of these spheres was verified with a micrometer as shown in Table 5.

Table 5 - Sample dimensions

Sphere	Diameter, μm
A	1991
B	2008
C	2004

Before treatment, the spheres were washed for 1hr in Piranha solution (30% H_2O_2:70% H_2SO_4) at 60-70°C before treatment. Once washed the spheres were stored in a sealed container filled with Nanopure water. All measurements were done at 20°C ± 0.5°.

A sphere was then fixed to the end of a glass hook, which was manufactured by the Virginia Tech glass shop, using Crytalbond™ 509 glue (Electron Microscopy Sciences). The sphere was then suspended in a solution of cetyltrimethylammonium bromide (C_{16}TAB) for two hours to create a hydrophobic surface.

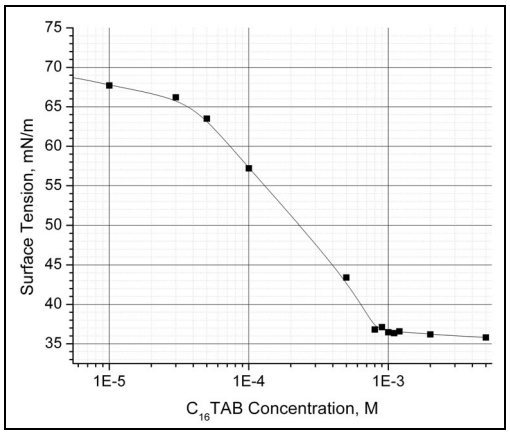

Figure 24 - Surface tension of C_{16}TAB aqueous solutions

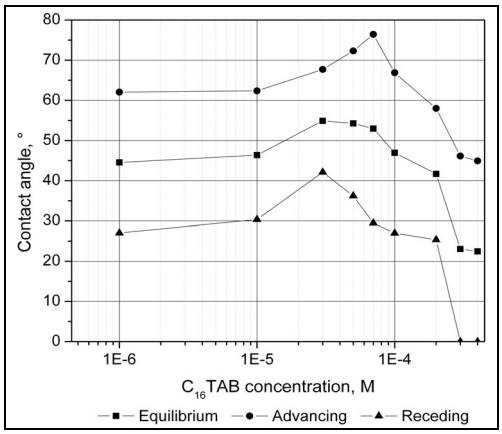

Figure 25 - Contact angle of C_{16}TAB aqueous solutions on glass

C_{16}TAB should reach equilibrium concentration on the glass surface after 1h (Yaminsky and Yaminskaya 1995). Solution concentrations ranged from 10^{-6}M to 10^{-3}M. Samples were first treated with the 10^{-6}M solution and force measurements were taken immediately after. Between measurements the samples were soaked in successively higher concentrations of C_{16}TAB. The purity of the C_{16}TAB (Fluka) was verified by testing the surface tension of a range of concentrations to identify the critical micelle concentration. The surface tension was measured using the same tensiometer equipped with a Du Nouy ring (Pt-Ir-ring made to DIN 53914-80 and ASTM D 971 specifications, also by KSV Instruments Ltd.). Figure 24 indicates a critical micelle concentration (CMC) of 9 x 10^{-4} M, which is in accordance with literature (Frank and Garoff 1996; Liu et al. 2001). The steady surface tension of the aqueous solution above the CMC also indicates an uncontaminated surfactant. The surface tension of pure water was measured at 72.6 mN/m.

Glass plates (Fisher Scientific) were cleaned and treated with C_{16}TAB using the same methods earlier described to obtain contact angle measurements for various concentrations. Advancing and receding contact angles were measured using the Wilhelmy plate principle with the KSV Sigma 70. The contact angles thus obtained can be seen in Figure 25. These measurements were also in agreement with literature (Janczuk et al. 1999).

The measured contact angles were also used to determine the surface free energy, γ_s, of the glass using equation [27] (Chibowski 2003).

$$\gamma_s = \gamma_l \left(\cos\theta_r - \cos\theta_a\right) \frac{\left(1+\cos\theta_a\right)^2}{\left(1+\cos\theta_r\right)^2 - \left(1+\cos\theta_a\right)^2} \qquad [27]$$

Where, γ_l is the surface tension of water, and θ_r and θ_a are the receding and advancing contact angle respectively.

To perform the force measurements, the sphere was suspended from the tensiometer above a flat bubble. The bubble was created using a PTFE rod, with a cone bored out in the center, connected to a syringe that provided the air for the bubble as shown in Figure 6. The bubble support sat in a rectangular glass cell filled with water on top of a mechanical stage that could be moved vertically at 1 mm/min to bring the bubble and particle into contact and then detach them.

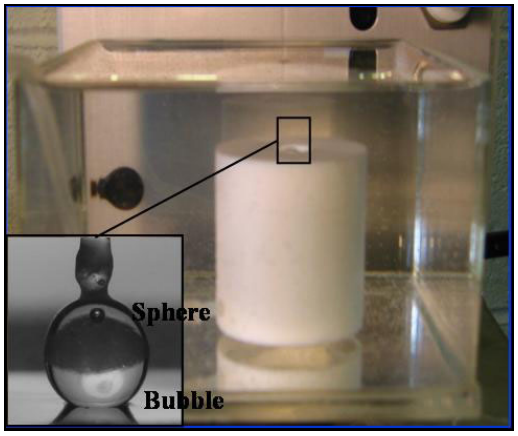

Figure 26 - Flat bubble apparatus

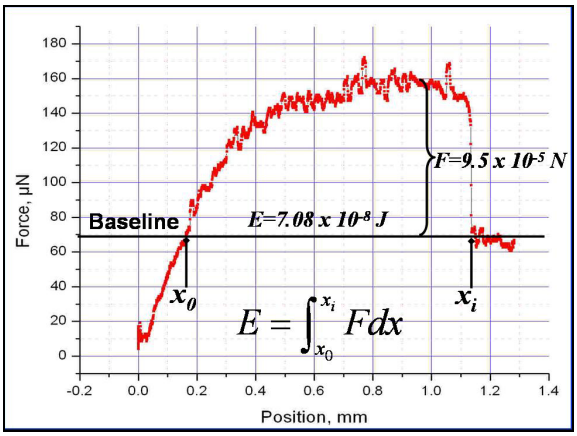

Figure 27- Detachment force curve

The tensiometer was connected to a computer to record force and distances every .25 s. The reported distance is the relative position of the mechanical stage. Although the actual position is not known, the distance traveled during the detachment process (used for energy calculations) is still recorded.

A typical output curve from the surface tensiometer is shown in Figure 27. The detachment force is measured as the difference between the maximum and the baseline. The baseline is the force at which the sphere is detached. This is the force exerted on the instrument from the weight of the sphere only. The energy is taken as the integral of the force applied across the distance from equilibrium to detachment. Equilibrium is shown in the figure as x_0. It is the point at which the bubble is neither pushing up nor pulling down on the sphere.

Results & Discussion

Detachment forces at increasing surfactant concentration are shown in Figure 28 for the three spheres. Sphere A measurements were stopped at 10^{-4} M because the sphere became unglued from the glass hook.

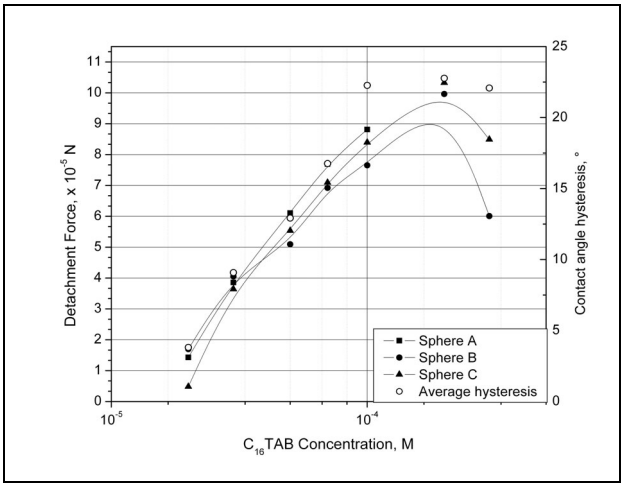

Figure 28 - Detachment force measurements of C_{16}TAB coated silica spheres

As expected, the force measurements showed good correlation between each sphere. The force of detachment was then used with equation [24] to calculate the advancing contact angle. Receding contact angle was calculated separately from radius of contact measurements at the equilibrium point. These measurements were taken from the images of the experiment. Force of detachment is closely related to contact angle hysteresis as shown in Figure 28. While the work of adhesion represents the work necessary to detach the particle once this detachment force has been reached.

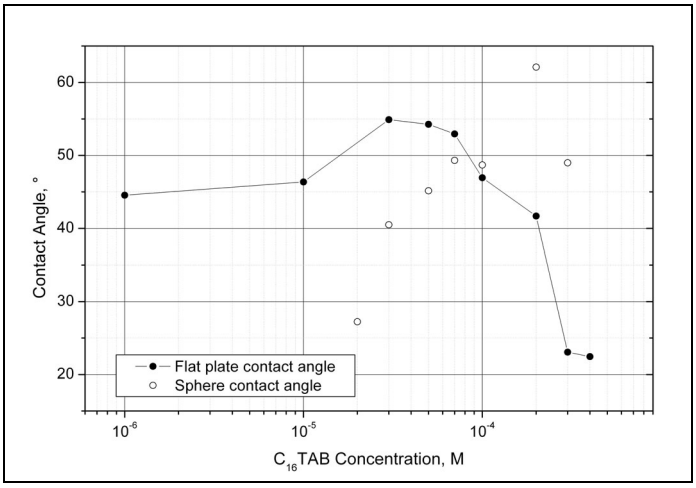

Figure 29 - Flat plate and sphere contact angle

As shown in Figure 29 the calculated contact angles differed considerably from the flat plate measurements. Some differences in contact angle based on the solid shape have been reported before (Preuss and Butt 1998b). The contact angle on a sphere can be 10° smaller for the same surface on a flat plate. This phenomenon was reported for low contact angle surfaces.

The dynamic nature of C_{16}TAB adsorption at the TPC line is also a factor explaining the difference in measurements on the sphere and flat plate. As concentration increases, the dynamic contact angle behavior may be explained by Gibbs' adsorption equation.

$$-\frac{d\gamma}{d\mu} = \Gamma \qquad [28]$$

Where μ is the chemical potential and Γ is the adsorption. The force on a solid partially immersed in water minus the buoyancy can be expressed as the wetting tension (Eriksson et al. 1996).

$$\tau = \gamma_{sv} - \gamma_{sl} \qquad [29]$$

Equation [29] can be substituted into equation [28] to obtain equation [30] (Yaminsky 1994).

$$-\frac{\partial\tau}{\partial\mu} = \Gamma_{sv} - \Gamma_{sl} \qquad [30]$$

Thus, the slope of the wetting tension isotherm represents the competition for adsorption of C_{16}TAB molecules at the solid-liquid and solid-vapor interface.

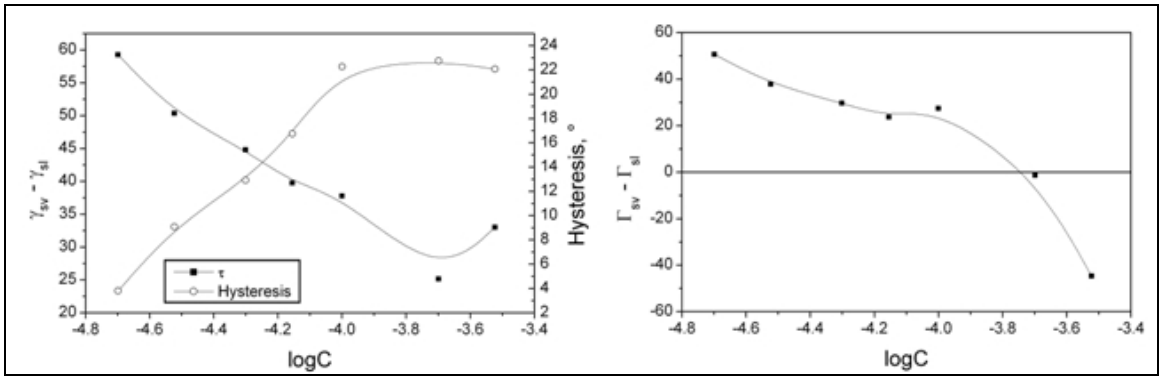

Figure 30 - (a) Wetting tension isotherm and (b) Adsorption difference isotherm

The wetting tension isotherm was graphed as shown in Figure 30(a) to find the slope of the line, which is shown in Figure 30(b). The derivative of the wetting tension isotherm does not produce the adsorption difference isotherm but is still useful as the sign of the derivative and the relative magnitude are still represented. The competition between solid-vapor and solid-liquid interface for C_{16}TAB adsorption explains the variation in contact angle and detachment force with increasing concentration. Hysteresis increases linearly with concentration until about 10^{-4}M. The linear relationship is reflected in the adsorption isotherm as the slope only decreases slightly until about 10^{-4}M. Beyond this point the slope magnitude increases sharply as the solid-vapor interface begins to adsorb less C_{16}TAB compared to the solid-liquid interface. As the adsorption difference approaches zero and becomes negative, the hysteresis plateaus and then begins to decrease.

When the sphere comes into contact with the bubble, and the TPC line spreads over the solid surface the C_{16}TAB molecules migrate out of the water onto the dry surface. This creates a high concentration gradient of surfactant molecules at the dry boundary, allowing the C_{16}TAB hydrophobic tails to escape the water. This accumulation creates a band of increased hydrophobicity on the sphere. These bands then create a surface more prone to pinning for subsequent experiments, thereby increasing hysteresis.

Hysteresis from surface domains

An atomic force microscope was used to produce images of C_{16}TAB coated silica surfaces. Silica wafers were coated with a range of C_{16}TAB concentration using the same procedure previously described. Silica wafers were used because they provide a very smooth surface (mean roughness was ≈ 0.2 nm) on which chemical heterogeneity could be observed. The sphere surface was too rough (50 – 75 nm roughness) to easily see C_{16}TAB molecules, which are only 20Å long. Figure 31 shows the AFM images which provide a qualitative justification for contact angle hysteresis. The patches on these images were about 20Å high which indicated that they were probably the beginning of the C_{16}TAB monolayer formation. As the concentration is increased, the domains seem to grow larger and more frequent. This provides local hysdrophobic sites for the TPC line to get pinned, which in turn leads to increased hysteresis.

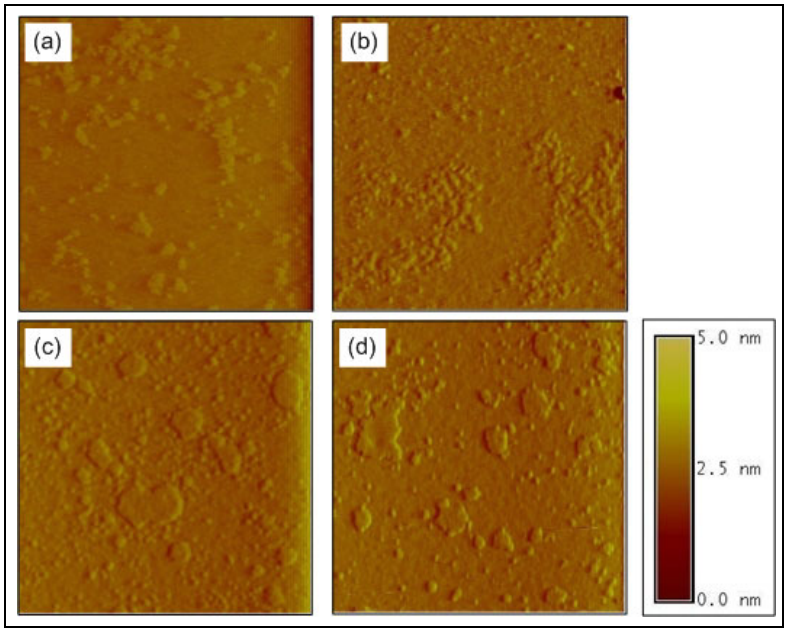

Figure 31 - AFM images of (a) $1x10^{-5}$M, (b) $3x10^{-5}$M, (c) $5x10^{-5}$M, (d) $1x10^{-4}$M C_{16}TAB coated silica wafer. Each square is 5µm x 5µm.

Energy calculations

The energy of detachment was compared with the work of adhesion calculated with equation [11]. The detachment force curve is split into two sections, the stretching or energy barrier, E_1, and the sliding, E_2. E_1 is the energy spent shifting the TPC line from

receding to advancing contact angle. Once the advancing angle is reached, then detachment may begin. E_2 is equivalent to the work of adhesion. The results of these calculations are displayed in Figure 32. The theoretical work of adhesion showed good correlation with measured energy. The difference between total energy of detachment and work of adhesion demonstrates the irreversibility of the bubble particle interaction.

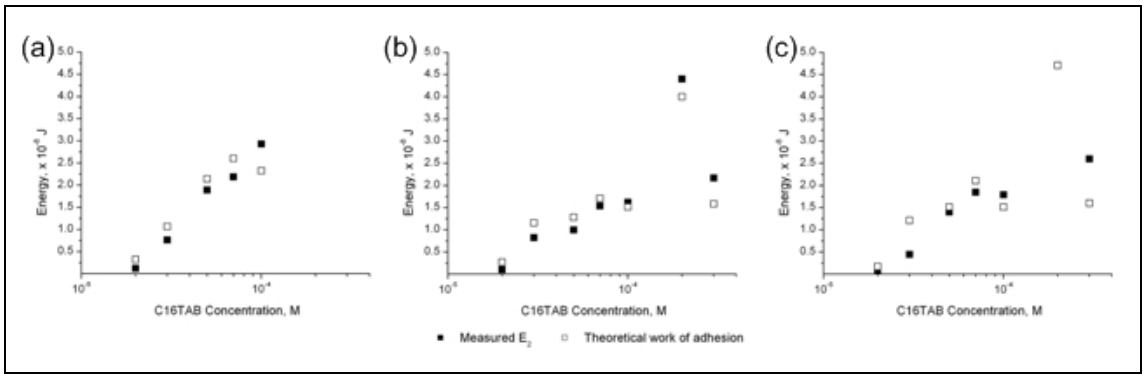

Figure 32 - Measured detachment energy, E_2, and theoretical work of adhesion for (a) Sphere A, (b) Sphere B, (c) Sphere C

Detachment Energy in Flotation

Figure 33 demonstrates the relationship between detachment energy and possible reagent usage in a flotation environment.

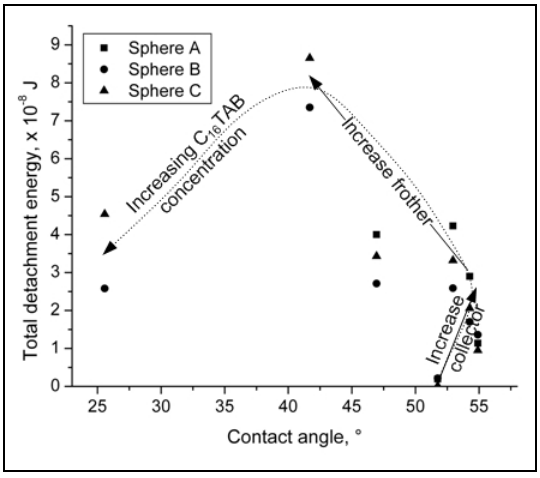

Figure 33 - Total detachment energy VS equilibrium contact angle

Increasing collector dosage increases the contact angle leading to higher detachment energies. Increasing frother decreases contact angle but this is compensated by the increase in bubble tensile strength. However, if surface tension is decreased too much, the bubbles are too strong and do not rupture easily to adhere properly to the hydrophobic particles.

Summary & Conclusion

Bubble-particle detachment energy was successfully measured as indicated by the good correlation with the theoretical work of adhesion. Total detachment energy is larger than the work of adhesion because the energy barrier for movement of the TPC line must be overcome before detachment will begin. The energy barrier is directly related to contact angle hysteresis. It is the energy spent shifting the TPC line from receding to advancing contact angle. The close relation between hysteresis and detachment force was also demonstrated.

Contact angle hysteresis is affected by the dynamic nature of C_{16}TAB adsorption at the solid-liquid-vapor interface. C_{16}TAB adsorption at the solid-vapor interface during sphere-bubble attachment and during Wilhelmy plate measurements created discrepancies between contact angle measurements at the same concentrations.

With increasing C_{16}TAB concentration, the contact angle of the sphere was increased while bulk solution surface tension was decreased. This clearly showed the careful balance between frother and collector dosages that must be optimized in coarse particle flotation.

References

Adamson, A. W. (1997). Physical Chemistry of Surfaces, J. Wiley, New York.

Chibowski, E. (2003). "Surface free energy of a solid from contact angle hysteresis." Advances in Colloid and Interface Science, 103(2), 149-172.

Eriksson, L. G. T., Claesson, P. M., Eriksson, J. C., and Yaminsky, V. V. (1996). "Equilibrium wetting studies of cationic surfactant adsorption on mica 1. Mono- and bilayer adsorption of CTAB." Journal of Colloid and Interface Science, 181, 476-489.

Frank, B., and Garoff, S. (1996). "Surfactant self-assembly near contact lines: control of advancing surfactant solutions." Colloids and Surfaces A: Physicochemical and Engineering Aspects, 116(1-2), 31-42.

Israelachvili, J. (1991). Intermolecular & Surface Forces, Elsevier Ltd., London.

Janczuk, B., Wojcik, W., and Zdziennicka, A. (1999). "Wettability and surface free energy of glass in the presence of cetyltrimethylammonium bromide." Materials Chemistry and Physics, 58(2), 166-171.

Liu, J.-F., Min, G., and Ducker, W. (2001). "AFM study of adsorption of cationic surfactants and cationic polyelectrolytes at the silica-water interface." Langmuir, 17, 4895-4903.

Preuss, M., and Butt, H.-J. (1998). "Measuring the Contact Angle of Individual Colloidal Particles." Journal of Colloid and Interface Science, 208(2), 468-477.

Sutherland, K. L. (1948). "Kinetics of the flotation process." J. Phys. Chem., 52, 394-425.

Yaminsky, V. V. (1994). "Thermodynamic Analysis of Solute Effects on Surface Forces. Adhesion between Silicates in Solutions of Cationic Surfactants." Langmuir, 10, 2710-2717.

Yaminsky, V. V., and Ninham, B. W. (1999). "Surface forces vs. surface compositions. Colloid science from the Gibbs adsorption perspective." Advances in Colloid and Interface Science, 83(1-3 SU -), 227-311.

Yaminsky, V. V., and Yaminskaya, K. B. (1995). "Thermodynamic analysis of solute effects on contact angles. Equilibrium adsorption of cationic surfactants at silica-vapor and silica-water interfaces." Langmuir, 11, 936-941.